University of Calgary

PRISM Repository **https://prism.ucalgary.ca**

The Vault Open Theses and Dissertations

2013-09-06

Development and Investigation of Micro Mechanical Machine Tools and Processes

Park, Chaneel

Park, C. (2013). Development and Investigation of Micro Mechanical Machine Tools and Processes (Master's thesis, University of Calgary, Calgary, Canada). Retrieved from https://prism.ucalgary.ca. doi:10.11575/PRISM/25643

http://hdl.handle.net/11023/929

Downloaded from PRISM Repository, University of Calgary

UNIVERSITY OF CALGARY

Development and Investigation of Micro Mechanical Machine Tools and Processes

by

Chaneel I. Park

A THESIS
SUBMITTED TO THE FACULTY OF GRADUATE STUDIES
IN PARTIAL FULFILMENT OF THE REQUIREMENTS FOR THE
DEGREE OF MASTER OF SCIENCE

DEPARTMENT OF MECHANICAL AND MANUFACTURING ENGINEERING
CALGARY, ALBERTA
SEPTEMBER 2013

© Chaneel Park 2013

Abstract

Micro-mechanical machining using diamond tools is advantageous to other micro-manufacturing techniques as it can create complicated geometric features with high precision, and it is applicable to a wide range of materials including polymers and metals. The effectiveness of manufacturing micro-scale features can be enhanced by understanding the process and interactions between the tools and materials.

Investigation of material properties with respect to the machining process is especially important when the material has unique mechanical properties such as polymeric carbon nanotube (CNT) nanocomposites with aligned CNTs and when the process itself is a unique such as an elliptical vibration machining (EVM) process. This study has sought to develop a micro indenter-scriber system for investigation of mechanical machining characteristics of the injection molded polymeric CNT nanocomposites, identifying parameters to model the micro scribing process. The study also aimed to develop a versatile EVM system with motion amplification without limiting the operation frequency to the natural frequencies of the system. The developed system was used to investigate its range of motion and effects of vibration frequency to reduce machining forces.

A custom micro indenter-scriber system was developed, capable of 3-axis nanometric displacements and 3-axis force sensing, along with a Berkovich diamond tool with known geometry. Polystyrene based multi-walled CNT – polystyrene (MWCNT-PS) composite samples at varying CNT concentrations (0, 0.5, 2.0 and 5.0 wt.%) were prepared through micro injection molding procedures to align CNTs in the composite. Using the custom indenter-scriber system, indentation and scribing experiments were performed to identify the indentation hardness,

modulus of elasticity and scribing forces in varying concentrations and orientations of CNTs.

Indentation experiments have found that CNT composite samples have increased hardness with small addition of CNTs (i.e. 0.5 wt.%); however, adding more CNTs (i.e. 5.0 wt.%) would result in decreased hardness. Scribing forces were revealed to have similar trends, showing the highest scribing forces at 0.5 wt.% of CNT concentrations but less at 5.0 wt.%. The orientation of CNTs also affected the forces, as higher forces were observed when scribing perpendicular to the CNT flow direction than scribing parallel to them. A micro scribing force model was proposed to predict forces from given material properties, then three unknown parameters, namely the shearing coefficient, the plowing coefficient and the adhesion friction coefficient were identified from experimental scribing tests. A relationship was established between three parameters with respect to the material properties, which would enable prediction of scribing forces from material properties.

To minimize forces in micro machining, a versatile EVM system was developed which consist of a diamond tool, two piezoelectric actuators, flexure joints and levers capable of amplifying vibrational motions. A mathematical toolpath generation algorithm was developed and compensated through experiments. Using the EVM system, experiments were performed at varying frequencies (i.e. 0, 1, 10 and 50 Hz) to measure the vertical and horizontal forces. It was found that increasing the vibration frequencies reduced the forces. Its surface pattern generation ability was also tested at a relatively high feed rate (300 μm/s) to examine whether the system can accurately fabricate dimples of 5 and 20 μm depths.

Understanding micro scribing force model of polymeric CNT nanocomposites provides fundamental understanding in the relationship of cutting forces and material properties, while the development of new EVM system and understanding of its mechanism provides a basis for

optimization of machining parameters of more accurate, precise and efficient micro mechanical machining. This knowledge will be applicable not only to conventional materials but to hard-to-cut materials such as glass, ceramics and polymeric CNT nanocomposites, providing accurate and economic methods to fabricate micro channels for biomedical applications, micro thermal exchanger, micro electromagnetic interference shield, micro optical lens and various functional surfaces with geometrically complex features.

Acknowledgements

I would like to express my gratitude to my supervisor Dr. Simon Park for his guidance through the course of my Master's program, his comments and remarks supported me in both academia and student life. I also thank the Natural Sciences and Engineering Research Council - Canadian Network for Research and Innovation in Machining Technology (NSERC CANRIMT) for their financial support and the Alberta government for the Queen Elizabeth II scholarship. In addition, I thank all my colleagues from Micro Engineering Dynamics and Automation Laboratory (MEDAL), especially Mr. Dennis Trieu, Dr. Mohammed Malekian, Mr. Golam Mostofa, Dr. Mehdi Mahmoodi and Mr. Shane Oh for their assistance in my studies. Finally, I thank my loving family for their love and support.

Table of Contents

List of Tables

List of Figures

List of Symbols and Nomenclature

A	Vertical amplitude of toolpath vibration
A_1, A_2	Vibration amplitudes of piezoelectric actuators
A_p	Projected area
a	Major radii of toolpath vibration
a_p, m	Power law constants of indentation unloading curve
B	Horizontal amplitude of toolpath vibration
b	Minor radii of toolpath vibration
C_1, C_2	Linear relationship constants
E	Modulus of elasticity of sample
E_i	Modulus of elasticity of indenter
E_r	Reduced modulus of elasticity
F	Force
F_a , F_b	Forces applied from actuators
F_C	Cutting force
$F_{FS,} F_{FP,} F_{FE}$	Friction forces of shearing, plowing and elastic recovery regimes
F_{max}	Maximum indentation force
$F_{NS,} F_{NP,} F_{NE}$	Normal forces of shearing, plowing and elastic recovery regimes
F_T	Thrust force
F_X , F_Y	Cutting force in x and y directions
F_{XE} , F_{YE} , F_{ZE}	Forces in x, y, z directions from elastic recovery regime

F_{XP} , F_{YP} , F_{ZP}	Forces in *x, y, z* directions from plowing recovery regime
F_{XS} , F_{YS} , F_{ZS}	Forces in *x, y, z* directions from shearing regime
f	Vibration frequency
G_1 ,G_2	Geometric constants of the EVM system
H	Hardness
h	Depth of cut
h_a	Height of material pile-up
h_c	Contact depth of indentation
h_{er}	Depth of elastically recovered material
h_m	Minimum uncut chip thickness
h_p	Depth of plastic deformation
h_R	Vertical height of blunt part of the tool
h_r	*x* - intercept of the tangent line of the indentation unloading curve
r	Tool edge radius
V	Feed rate
α	Tool rake angle
α_e	Effective tool rake angle
Γ	Mathematical gamma function
ε	Indentation geometric constants
η	Effective angle between the feed direction and the normal vector of the surface
η_c	Angle between the feed direction and the normal vector of the surface

θ	Berkovich tool geometric angle
$\kappa_1, \kappa_2, \kappa_3, \kappa_4$	Abbreviated functions of EVM input parameters
κ_p	Plowing coefficient
κ_s	Shearing coefficient
λ	Empirical constants for toolpath calibration
μ_a	Adhesion friction coefficient
ν_i	Poisson's ratio of indenter
ν_s	Poisson's ratio of sample
ρ_e	Elastic recovery ratio
φ	Phase angle
χ	Tilt angle of elliptical toolpath
ω	Angular vibration frequency

CHAPTER 1. INTRODUCTION

Scientific and engineering advancements in micro-scale and nano-scale technologies have led to increasing demand for efficient fabrication of micro-sized components. Examples include micro fluidic channels, applied lab-on-chip devices, as well as functional surfaces with micro/nano-sized features, bearing surfaces with reduced friction, hydrophobic surfaces and optical lenses. Microelectromechanical system (MEMS) sensors and actuators are also good examples of products requiring high-precision micro-sized parts.

For commercial products, techniques based on semi-conductor processing techniques are very popular, involving photo-etching of target materials through chemicals and dry processes [Chae et al. 2006]. Other methods, such as laser, ion beam and electro discharge machining (EDM), are also practised and investigated. Another fabrication technique is micro mechanical machining, which uses scaled miniature tools to remove and/or deform the workpiece through mechanical forces.

Micro mechanical machining has the same unique advantages that conventional mechanical machining has over other techniques. First, it is more economical, as it does not require large initial setup costs, a continuous supply of expensive masks or a large amount of electrical power compared to the EDM, photolithography or laser machining processes. Mechanical machining is also time efficient, especially in the fabrication of individual components rather than producing large batches of the same products. This method is applicable to a wide range of materials, regardless of their chemical reactivity, such as composites, metallic alloys, polymers and ceramics. Furthermore, mechanical machining is capable of fabricating

complex three-dimensional (3-D) shapes with relative ease, whereas other techniques may require extensive step-by-step procedures to have 2.5-D results. With its unique advantages and the recent developments of sufficiently small machine tools and high-precision control methods, mechanical machining has become a viable micro scale manufacturing technology.

The paradigms of conventional macro mechanical machining, however, cannot be transferred directly to micro mechanical machining, as some of the issues that are considered negligible in the macro scale have significant effects in micro machining. The tool edge radius is considered ideally sharp in macro-sized conventional cutting, resulting in material removal in the form of chips (i.e. shearing). In the realm of micro cutting, the depth of cut is often comparable to or smaller than the tool edge radius, and the rake angle of the tool edge and corresponding parameters in the cutting mechanisms are changed. Therefore, the plastic deformation of materials, called plowing, may occur instead of shearing, leaving pile-ups and built-up edges. Moreover, the microstructure of materials, such as the grain size and their boundaries, or the existence of filler materials may cause anisotropy in the material properties, thereby influencing micro machining process. Micro mechanical machining requires further studies based on the knowledge gathered from conventional machining processes.

1.1 Motivations

Considering the size effects, it is very important to have a thorough understanding of the mechanisms of the micro mechanical machining process. Two different aspects of micro mechanical machining can be studied: the characteristics of the specific materials under micro mechanical machining conditions; and, specific micro mechanical machining processes with improved machining characteristics. In this study, both aspects are investigated: the micro

mechanical cutting of polymer nanocomposites with multi-walled carbon nanotubes; and, the micro elliptical vibration machining process.

1.1.1 Polymeric CNT Nanocomposites

Researchers have mixed carbon nanotubes (CNTs) with polymer to form composites, not only with improved mechanical properties, by increasing the modulus of elasticity and tensile strength [Spitlasky et al. 2010], but also with electrical and thermal conductivity by forming conductive networks of CNTs inside the composite [Abbasi et al. 2010].

Polymeric CNT nanocomposites are applicable as structural materials for automobiles and airplanes, due to their high strength-to-weight ratios. Their high electrical conductivity makes them appropriate materials for EMI shielding and anti-static packaging. They can also be used as heat sinks for microchips, dissipating heat through thermally conductive CNTs.

Injection moulding of polymeric nanocomposites is often used to fabricate a large quantity of complex components. Since the injection moulding process exhibits high shear stress in the melt flow direction, the CNTs become partially aligned in the flow direction in the fabrication of polymeric CNT nanocomposites. Arjmand and others [Arjmand et al. 2011, Mahmoodi et al. 2012] found that a higher degrees of alignment of CNTs results in less interconnection between CNTs, increasing the electrical percolation threshold. It was also found that materials are more conductive if the electrical conductivity is measured parallel to the CNT alignment rather than being measured perpendicular to the alignment in both polycarbonate [Arjmand et al. 2011] and polystyrene [Mahmoodi et al. 2012] based nanocomposites. The anisotropy caused by the CNT alignment is not limited to electrical properties; it also affects the thermo-mechanical properties of the composites.

The dispersion of CNTs is largely dependent on the mould shape; thus, complex

geometries cannot be achieved through injection moulding without the loss of desired material properties [Mahmoodi et al. 2012]. A micro mechanical machining technique can be applied after batch production through micro injection moulding, fabricating complex geometries through material removal with minimal effects on CNT distributions and alignments.

There have, however, only been a limited number of works on micro mechanical machining characteristics of aligned polymeric CNT composites. Samuel and others modelled and investigated micro cutting of CNT-polycarbonate (PC) composites using finite element analysis [Samuel et al. 2008] and micro machining response of CNT nanocomposites [Samuel et al. 2010]. Also, there was experimental investigation of machinability on CNT-polystyrene (PS) composites using micro milling [Mahmoodi et al. 2013]. While micro milling is a viable micro mechanical machining technique, it is difficult to identify parameters related to the more fundamental modelling of micro mechanical cutting processes.

For experimental study of mechanical properties and machining characteristics of CNT nanocomposites with flow-induced CNT alignments through injection moulding, micro mechanical scribing is appropriate. This scribing technique can provide fundamental knowledge of the mechanical cutting process, such as the friction coefficient; and, a single-point diamond tool used in the scribing can be utilized in the identification of material properties. Among the studies previously reported, there was no previous study that investigated the material properties of polymer nanocomposites and machining characteristics together, especially with respect to the orientation of CNTs. This study provides quantified parameters that define the relationship between material properties and scribing characteristics with respect to CNT loads and orientations inside polymeric CNT nanocomposites.

1.1.2 Elliptical Vibration Machining

Studying the material-specific machining characteristics and adjusting the machining parameters is one method to improve the machining efficiency. However, this approach requires studying of each individual material for optimization, and it cannot really solve the issue of high forces associated with the micro cutting process. One of the main challenges in micro machining is the reduction of cutting forces in order to keep the fragile tools from severe wear and breakage and to minimize large deflections, which may violate part tolerances. Tool fragility often results in conservative process settings with a chip thickness less than the critical value, resulting in an increasingly large negative rake angle and elastic-plastic deformation [Waldorf 2006].

In order to solve this issue, Shamoto and Moriwaki introduced a new technique called elliptical vibration machining, where the tool travels in an elliptical locus as the materials are fed into the tool, instead of vibrating in a one-dimensional linear vibration. This significantly reduces the required force for machining and improves the surface finish [Shamoto and Moriwaki 1994]. Due to its rotational motion in two dimensions, it is classified as two-dimensional (2-D) vibration-assisted machining.

Elliptical vibration cutting proved its usefulness in many applications; and, new ways of applications have been developed as well. However, Jin and Murakawa reported that this process is more suitable for micro cutting operations, due to its complicated vibration mode [Jin and Murakawa 2001]. In other words, the elliptical vibration machining (EVM) method would be suitable for probe-based nano and micro mechanical machining where the amplitude of the vibration is small. Studies of the adoption of EVM into micro/nano mechanical machining have recently begun.

There have been different experimental setups developed in the relatively short history of

EVM, but they can be largely categorized into two types: resonant and non-resonant EVM systems. Resonant EVM systems, as the name indicates, utilize the resonance of a system at natural frequencies to amplify the vibration exerted by piezoelectric actuators [Shamoto and Moriwaki 2002]. The downside of this design is that the operational range of the vibration frequency is limited to the modal frequency of two vibrational directions.

Non-resonant EVM systems have mechanical linkages that translate linear actuations into elliptical motion [Cerniway 2001]. They can operate over a varying range of frequencies; however, the system involves more parts and moving joints, where heat accumulation and material fatigue can be limiting factors under continuous exposure to high frequencies. In order to study the EVM mechanism in depth, it is necessary to have a versatile EVM system that is free of such disadvantages.

1.2 Objectives

For successful implementation of micro mechanical machining, it is important to further elucidate the mechanism behind its process beyond the conventional machining theories. Therefore, material properties and machining characteristics need to be investigated, in terms of micro mechanical machining, which includes the analysis of force and mechanistic modelling based on input parameters.

In this study, two different processes of micro mechanical machining, namely micro scribing of polymeric CNT nanocomposites with aligned CNTs and micro EVM were examined. Custom experimental setups were developed for each cutting process, in order to perform the corresponding machining processes and measure the dynamic forces at the same time. Measurements of the experimental forces are fundamental data in the understanding of

machining processes and can be used along with the mechanistic model to find the material and process-specific characteristics.

1.2.1 Objective for MWCNT-PS Micro Scribing

Multi-walled carbon nanotube and polystyrene (MWCNT-PS) nanocomposites were used in this research; however, the methodologies in this study are applicable to other polymeric CNT nanocomposites. The objective of this part of the research was the development of an indenter-scriber system, and to find the material properties of the MWCNT-PS nanocomposites and their scribing characteristics at varying concentrations of MWCNTs and feed directions. This would ultimately explain the relationships between scribing forces and material properties due to CNT loads in the mechanistic force model. To achieve this objective, the following steps were taken:

i. *Development of the micro indenter-scriber system:*

If mechanical machining characteristics in the macro scale cannot be translated directly into the micro mechanical machining, an understanding of material properties in the realm of microns is required. It has been reported that material properties specific to micro-sized areas are different from bulk material properties: they tend to show larger hardness and modulus of elasticity than bulk materials.

With the micro scribing process and its mechanistic force modelling, the micro indentation technique can be applied utilizing the same single-point diamond tool used in the scribing. Therefore, a combinational system of a micro indenter and scriber was developed in-house. Unlike atomic force microscopes, where relatively lengthy calibration is required and the maximum force is limited by the cantilever stiffness, the developed micro indenter-scriber system has a rigid diamond tool. A three-axis nanostage and a high-resolution force sensor were controlled by and data acquired through a

computer, allowing for the continuous measurement of forces for both the micro indentation and scribing processes.

ii. *Identification of material properties of MWCNT-PS though micro indentation:*

Using the developed indenter-scriber system, micro indentation experiments were conducted on the MWCNT-PS samples, performing cycles of loading and unloading tool displacement and recording the corresponding forces. The analysis was based on Oliver and Pharr's method [Oliver and Pharr 1994] with consideration of the sink-in effect and elastic recovery, given the hardness and modulus of elasticity of MWCNT-PS at varying CNT concentrations.

iii. *Experimental force analysis at varying CNT concentrations and feed directions:*

Micro scribing forces were measured during scribing experiments of the MWCNT-PS materials. Concentrations of CNT were varied along with the feed directions, as the materials were fed in parallel and perpendicular directions with respect to the flow direction of molten polymer in the injection molding process. Experiments were conducted twice, with the first set of experiments orienting the tool, so that the rake face was symmetric; and, the second set of experiments had the tool oriented so that the rake face was asymmetric.

With the first set of experiments, the horizontal cutting and vertical thrust forces were measured, and the apparent friction coefficient was determined from the ratio of these forces. This provided valuable information on the general trend of the scribing of MWCNT-PS nanocomposites. In the second set of experiments, three axes of forces were measured due to the asymmetry, F_x, F_y, and F_z, which were used to establish the mechanistic scribing force model.

iv. *Establishing a mechanistic force model and identification of cutting coefficients:*

A novel micro scribing mechanistic force model was developed, considering material shearing, plowing and elastic recovery. The model can be used to predict forces based on the material properties found from indentations, given the shearing, plowing and adhesion friction coefficients. These three parameters were determined from experimental analyses of scribing forces, fitted to verify the validity of the model.

1.2.2 Objectives for the Development and Investigation of an EVM System

Researchers have developed unique EVM systems designed specifically for their studies. In this study, a versatile EVM system was proposed to avoid the disadvantages of resonant and non-resonant systems. The system operates in all ranges of vibration frequency, similar to non-resonant systems, but is capable of amplifying the range of motion as with resonant systems. With this versatility, various experiments could be performed to contribute to a further understanding of EVM mechanism. The objectives of the EVM system development and the experimental investigations using the developed EVM system were:

i. *Development of the EVM system and its control algorithm:*

A novel EVM system was developed, capable of mechanical amplification of actuations through the concept of leverage and flexural hinges, generating elliptical motions in a wide range of amplitudes and frequencies. It could create tool paths in various aspect ratios and angles, as well as geometries other than a circle or an ellipse. The system's amplification ratios were experimentally verified. Its control algorithm was mathematically predicted based on ideal conditions and equations were compensated using parameters obtained from experiments.

ii. *Experimental investigation of the EVM process and verification of surface pattern*

Studies on the EVM process revealed that it reduces the applied forces compared to orthogonal scribing where no vibration is applied. The developed EVM system was tested at varying frequencies and verified the force reduction effects. It was also tested at a relatively high feed rate to confirm that it could create surface patterns with accuracy and measure generated surfaces.

Following the given objectives, a thorough understanding of micro mechanical machining is obtained in terms of the relationship between materials, process parameters and resulting forces. Development of the mechanistic scribing force model of MWCNT-PS provides quantified relationship for scribing of polymeric CNT nanocomposites. The development of EVM system provides a required tool for future studies in comparative analysis of existing force models, ultimately leading to the development of a vibration assisted cutting force model. The developed tool is utilized for experimental observation of force reduction effects at varying vibration frequencies, verifying its capability as an experimental apparatus to study EVM in depth.

1.3 Thesis Organization

The thesis consists of five chapters, and the remainder of the thesis is organized as described in the following paragraphs.

Chapter 2 provides a review of the literature related to micro mechanical machining with a specific focus on the machining of polymeric CNT nanocomposites and the EVM process. In the first section of the chapter, the material properties and mechanical machining characteristics of CNT nanocomposites are described. The next section provides an introduction to the EVM

technique with a brief history, its benefits and the different types of EVM applications.

Chapter 3 describes the scribing experiments and modeling of forces using the single point diamond tool. The development of a new micro indenter-scriber system is presented. The system's different parts are described in detail, with explanations as to why they are implemented. An investigation of the diamond tool used in the experiment is also included. Micro indentation and scribing experiments are described. The results are discussed in comparison to other studies and material properties obtained through the different methods. With the results from the indentation and scribing sections, the mechanistic scribing force model is proposed and described in detail, and its relevance is discussed.

The development of a novel EVM system is described in Chapter 4. Its design and the final product are described, and experimental results are presented that confirm its range of motion. The control algorithm of the developed system is provided, and experimentally obtained errors are studied and compensated for. The EVM system is applied in a comparative analysis of orthogonal cutting and EVM processes. The EVM technique is utilized with varying frequencies and feed rates, and the resulting forces are analyzed. Surface patterns are fabricated using the EVM technique at relatively high feed rates, and the resulting geometries are scanned and analyzed.

Chapter 5 presents the conclusions of this study, and the novel contributions of this study to the knowledge of the micro mechanical machining are described. The assumptions and limitations of the study are included, and possible future works that further improves this work are discussed.

CHAPTER 2. LITERATURE SURVEY

In this chapter, the literature of topics relevant to this study are presented. First, material properties of polymeric CNT nanocomposites with respect to CNT loads and orientations, and their characteristics under micro mechanical machining are introduced. In the later sections, current theories explaining the elliptical vibration machining (EVM) process, its benefits and applications are described. It is explained what are the currently achieved and what kind of further investigations are required in motivation of this study.

2.1 Studies on Micro Scribing of Polymeric CNT Nanocomposites

A novel contribution toward understanding of micro scribing of polymeric CNT nanocomposites can be achieved by building a strong foundation of knowledge. In this section, superior material properties of CNTs are introduced along with the description of how CNTs could improve material properties composites when they are added as filler materials. Electrical, thermal and mechanical properties of polymeric CNT nanocomposites are discussed in relation to CNT loadings and orientations based on other studies, emphasizing the importance of studying micro mechanical machining characteristics of polymeric CNT nanocomposites.

2.1.1 Polymeric CNT Nanocomposites

Carbon nanotube has superior mechanical properties and it has been reported repeatedly by researchers. Young's modulus of multi-walled carbon nanotubes (MWCNTs) can reach up to 1 TPa [Yu et al. 2000] while its highest tensile strength was reported to be approximately 150

GPa [Demczyk et al. 2002]. On top of the exceptional mechanical properties, CNTs also possess superior thermal and electric properties. They are thermally stable up to 2800 ℃ in vacuum, thermal conductivity about twice as high as diamond, and electric-current-carrying capacity 1000 times higher than copper wires [Collins and Avouris 2000]. Such exceptional material properties combined with high aspect ratio of approximately 200 (for MWCNT) makes them as a suitable filler material to form composites and to enhance material properties of matrix material. While there are varying types of CNT nanocomposites where ceramics [Xia et al. 2008] or metals [Chen et al. 2003] are used as the matrix of the composites, the majority of CNT nanocomposites are polymeric CNT nanocomposites, as they are suitable for mass production, more economic and shows dramatic change in material properties. Polymers are mostly known for their low thermal and low electrical conductivity. There have been numerous reports on how addition of CNT fillers to polymer forms polymeric CNT nanocomposites with enhanced properties in mechanical, thermal and electrical aspects. Researchers were first interested in utilizing CNT's superior mechanical properties in polymeric nanocomposites. Qian and others compared the tensile strength and modulus of elasticity of MWCNT-PS to the pure polystyrene. With only 1 wt.% loads of MWCNT homogeneously dispersed in polystyrene matrix, the tensile strength has increased from approximately 12.8 MPa to 16.0 MPa, while modulus of elasticity increased from 1.19 GPa to 1.62 GPa. It requires approximately 10 wt.% of carbon fiber to be added to polystyrene to achieve the same extent of tensile strength and modulus of elasticity that 1 wt.% of MWCNT could achieve, due to the very high aspect ratio (ratio of length over the diameter) CNT has [Qian et al. 2000]. Similar results have been reported with use of single-walled CNTs (SWCNT) and MWCNTs as fillers and polystyrene (PS), polyethylene (PE), poly-methyl methacrylate (PMMA), polyvinyl alcohol (PVA) and polypropylene (PP) as matrix [Spitlasky et

al. 2010].

It was also reported that addition of CNT increases wear resistance and reduces the friction coefficient. Yang and others reported that addition of SWCNTs in to polystyrene increased micro-hardness, thereby reducing the wear rate. It is interesting to note that the micro-hardness of the composite was at the highest at 1.5 wt.% of CNT load; then decreased as more CNTs were added [Yang et al. 2005]. It was not explained in this paper but similar tendency was observed and explained by Samuel and others. It was explained that increased concentration of CNTs in the polymer matrix creates stress concentrations due to agglomeration of CNTs at the interface between the polymer and CNTs, resulting in easier crack propagations [Samuel et al. 2009]. Yang and others also observed a reduction in friction with increased load of CNTs, where CNTs act as dry lubricant [Yang et al. 2005].

Addition of CNTs also introduces electrical and thermal conductivity to the normally non-conductive polymers. Biercuk and others reported that, at the room temperature, the thermal conductivity of SWCNT-epoxy nanocomposite with 1 wt.% of CNTs was increased by 125% in comparison to the pure epoxy, as CNTs form a conductive network inside the polymer matrix. Such conductivity is three times larger than that of carbon fiber-epoxy composite with 1 wt.% of carbon fibers [Biercuk et al. 2002]. Electrical conductivity was also increased with addition of CNTs. For example, Chang and others achieved electrical conductivity of the composite of approximately 1 S/m by adding 1.5 wt.% of SWCNTs to the polystyrene matrix with electrical conductivity of 10^{-10} S/m [Chang et al. 2006]. Polymeric CNT nanocomposites achieved such a high conductivity with only a small loading of CNTs. With their inherent characteristics such as the low weight, low cost and optical clarity in addition to its electrical properties, it has huge potential in applications to the transparent conductive coatings, electrostatic dissipation,

electrostatic painting and electromagnetic interference shielding [Spitlasky et al. 2010].

2.1.2 Effects of CNT Alignments in Polymeric CNT Nanocomposites

The electrical and thermal conductivities are dependent not only on the matrix material but they are also heavily dependent on the dispersion and alignment of CNTs. As early as 2002, Thostenson and Chou have achieved CNT alignments by using a micro scale twin-screw extruder, where large shear forces applied during extrusion aligns CNTs inside the polystyrene matrices. They have observed approximately 3.5 GPa of storage modulus with aligned CNTs in comparison to the 2.5 GPa of storage modulus with randomly oriented CNTs [Thostenson and Chou 2002]. There are different methods to align CNTs in a polymer matrix such as the use of the high strength magnetic field [Kimura et al. 2002] but the flow-induced shear strength is used most commonly, since it occurs naturally during the injection moulding process, one of the most cost effective manufacturing methods in fabrication of polymeric components.

Abassi et al. [2010] produced composite of polycarbonate (PC) and MWCNTs in various ways: compression molding, conventional and micro injection moldings in disk and dog-bone shapes. They compared the resulting alignment of CNTs through Raman spectroscopy and TEM analysis, and found that micro injection molded dog-bone shape samples exhibit the highest degree of CNT alignments. They also observed that the higher degree of alignment of CNTs would result in lower electrical conductivity [Abassi et al. 2010].

Based on Abassi and others' work, Arjmand and others have investigated on the electrical properties depending on CNT alignment. They prepared MWCNT-PC samples using compression and micro injection molding processes. For the micro injection molded samples, they measured electrical conductivity in parallel and perpendicular to the CNT alignment. As a result, it was found that the randomly distributed CNTs (i.e. compression molded

nanocomposites) still have the highest electrical conductivity while the electrical conductivity was at its lowest when measured in the perpendicular direction to the CNT alignment. A higher degree of CNT alignment results in larger distances between CNTs than random distribution, resulting in the higher percolation threshold and electrical resistivity [Arjmand et al. 2011].

Mahmoodi and others have applied similar experiments using MWCNT-PS samples where degree of CNT alignment was varied by changing processing conditions in micro injection molding as well as mold geometries. They have also observed that electrical conductivity was lower when the CNT alignment was increased. The electromagnetic interference shielding properties were also measured, and they have found out that higher degree of alignment increases reflectivity but decreases absorption of electromagnetic waves [Mahmoodi et al. 2012].

Numerous studies have confirmed that CNT alignments in polymeric CNT nanocomposites play an important role in giving them unique anisotropic properties. However, the control of alignment is largely dependent on the geometries of injection molding cavities, runners and gates. Micro mechanical machining is an adequate method for post-processing of polymeric CNT nanocomposites, as it may achieve highly accurate and complex features without disturbing the CNT alignments during the process.

2.1.3 Mechanical Machining Characteristics of Polymeric CNT Nanocomposites

There has been only a limited number of works on micro mechanical machining characteristics of aligned polymeric CNT composites. Samuel and others simulated and modelled micro cutting of CNT-polycarbonate (PC) composites using finite element analysis (FEA). They observed that the shear strength for failure in CNT composites is low and reasoned that it is due to stress concentrations near the CNT-polymer interfaces. They also suggested that the high heat transfer rate of CNTs likely prevented material build-up, as the process becomes more shearing

dominant than plowing as the heat dissipates quickly [Samuel et al. 2009]. In a simulation study of cutting MWCNT-PC with aligned CNTs, they have concluded that cutting the sample in the cross-flow (perpendicular to the CNT alignment) direction would result in increased cutting forces and relatively rough surface due to the CNT pull-outs. However, this was limited to the cutting with highly positive rake angle. If a tool with negative rake angle is used, their simulation shows that CNTs are bent and not pulled out after cutting [Samuel et al. 2010].

Mahmoodi and others have performed micro milling experiments on MWCNT-PS samples with aligned CNTs. In this study, they performed fully immersed milling, where the tool was fed in-flow and cross-flow to the CNT alignments. Their experiments showed that the cutting coefficients were higher when the milling tool was fed in the in-flow direction instead of the cross-flow direction. This was mainly due to the fact that the actual cutting is occurring in the tangential vector of the rotation, which is generally perpendicular to the tool feed direction [Mahmoodi et al. 2012].

Investigation of micro milling of polymeric CNT nanocomposites may have more immediate application in the industry, however, scribing experiments provide more fundamental knowledge of the tool – material interactions. Therefore, the objective to establish a mechanistic force model of micro scribing of polymeric CNT nanocomposites with CNT alignments has great importance as a foundation for the modeling micro mechanical machining.

The elliptical vibration machining is one of the micro mechanical machining techniques that the understanding of the micro scribing process can be transferred to, where a single point diamond tool is implemented in dynamic motion. Prior to the incorporating knowledge of both techniques, a more basic understanding of what EVM is and how the process can be implemented is required, as introduced in the following section.

2.2 Studies on the EVM

In the realm of traditional orthogonal cutting, researchers have studied how to improve the efficiency of machining in various ways. One of the main challenges is to reduce cutting forces in order to protect the fragile tools from severe wear and breaking, and minimizing large deflections which may violate part tolerances. Tool fragility often results in conservative process settings with a chip thickness less than the critical value, producing in an increasingly large negative rake angle and elastic-plastic deformation [Waldorf 2006]. A method called vibration assisted machining was introduced to reduce cutting force and thereby improving overall machining efficiency.

Before 1950s, vibration during machining, often called chatter, was to be avoided at all cost. However at the late 1950's, applying controlled vibration to assist machining process was introduced by researchers [Skelton et al. 1968]. These first generation of vibration assisted machining applied vibration in parallel to the cutting direction, separating the tool from the chip in each cycle of vibration, reducing friction between the tool and the chip, ultimately reducing the cutting force [Kumabe et al. 1989; Moriwaki and Shamoto 1992; Jin and Murakawa 2001]. Since the vibration is applied in linear fashion, this is often classified as 1-D vibration assisted machining.

Furthermore, Shamoto and Moriwaki introduced elliptical vibration cutting, where the tool rotates in an elliptical locus as materials are fed into tools instead of one dimensional linear vibration, significantly reducing required forces for machining and improving surface finish [Shamoto and Moriwaki 1994]. Due to its rotational motion in two dimensions, it is classified as 2-D vibration assisted machining.

The elliptical vibration machining can be described in the three different stages in terms

of the position of the tools, which again defined by the horizontal velocity and vertical velocity of tool relative to the workpiece feed rate. At first, the horizontal speed of the tool exceeds the workpiece feed rate *V*, thus there is no contact between the tool and the sample. This is where the tool is away from the workpiece materials. As the vibration is applied, the horizontal speed of the tool becomes negative with respect to the workpiece feed direction, and vertically moving downward to apply cutting and thrusting force. This is where the greatest amount of cutting and thrust forces are applied, as the tool cuts into the workpiece materials. At the third stage, the vertical speed of the tool in the positive direction exceeds the chip flow speed, thus the friction between the tool and the chip assists in chip flow. During this process the tool assists the chip flow and moves away from the workpiece materials.

It is possible to control the cutting depth and force applied during the machining process by adjusting the vibration speed ω, the horizontal amplitude of vibration *A*, the vertical amplitude of vibration *B*, and the workpiece feed rate *V*. The schematic of fundamental elliptical machining is shown in Figure 2.1.

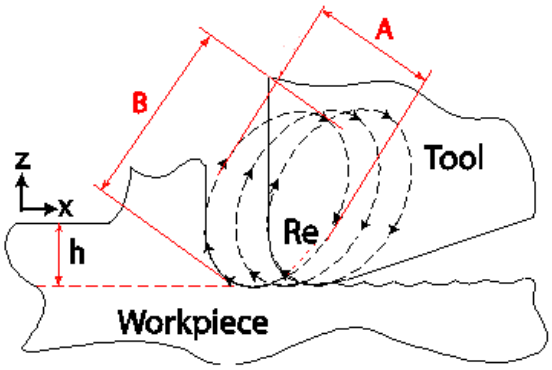

Figure 2.1 Schematic of elliptical vibration machining (EVM)

Elliptical machining is characterized by vibrating the tool in the x and y axes. The equations that describe the tool position relative to workpiece can be written as:

$$x(t) = -A\cos(\omega t) + Vt$$
$$z(t) = -B\sin(\omega t) \tag{2.1}$$

where x and z are the instantaneous positions, A and B are the amplitudes of the tool vibrations in the X and Z directions respectively, ω is the angular frequency of vibration, and V is the feed rate.

Since the main benefit of vibration machining is the reduction of forces during the cutting process, it is important to measure and analyze dynamic forces resulting from elliptical vibration machining. Ma and others [Ma et al. 2004] performed cutting experiments on an aluminum workpiece using a carbide tool, and compared the results from elliptical vibration machining to the average thrust forces obtained from the ordinary cutting (traditional turning) and conventional vibration cutting (1-D vibration assisted machining). They reported that elliptical vibration machining experienced significantly reduced thrust forces, which was at 2% of thrust forces obtained from traditional turning and 20% of thrust forces obtained from 1-D vibration assisted machining [Ma et al. 2004], as shown in Figure 2.2.

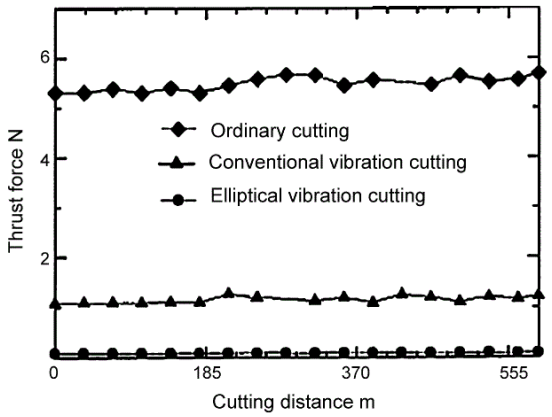

Figure 2.2 Comparison of average thrust forces [Ma et al. 2004]

There are several ideas suggested to explain the reduced cutting and thrust forces observed during the elliptical vibration machining; however, a comprehensive force prediction

model has not been established yet. Although, there are few researches that had been done regarding this issue, and it has been reported that the geometry of the elliptical tool path, frequency of the vibration and the feed rate are determining factors [Brinksmeir and Glabe 1999].

Shamoto and Moriwaki explain that such dramatic decrease in thrust force during elliptical vibration machining is due to the reduction in friction forces between the tool rake face and the chip [Shamoto and Moriwaki 1994]. When the vertical speed of the tool exceeds the chip flow speed, the friction between the tool rake face and the chip assists the chip, or 'pulls up' the chip. At extreme cases, Shamoto and Moriwaki even reported that the thrust force being negative during this 'pull up' process [Shamoto and Moriwaki 1994]. In the same manuscript, they performed elliptical vibration cutting at different frequencies (f = 0.12, 0.40, 1.20, 6.00 Hz), and reported that as the vibration frequency increases, both cutting (denoted as the principal force in their manuscript) and thrust force decreases. Being able to reduce machining forces by increasing the vibration frequency provides that machine feed rate can be maintained or even increased while controlling the machining force under the critical level to avoid any excessive tool wear or burr formation [Shamoto and Moriwaki 1994].

Cerniway also investigated dynamic forces during elliptical vibration machining [Cerniway 2001]. His work was distinguishable from Shamoto and Moriwaki's; the ratio of the depth of cut per vertical vibration amplitude was very small ($h/B < 1$) compared to that of Shamoto and Moriwaki's ($h/B \approx 3$). He kept his vibration frequency at 10 Hz. According to his manuscript, cutting force was reduced by 80% and thrust force was reduced by 48%. This is somewhat different from Shamoto and Moriwaki's result, but it is understandable since the tool path for Cerniway's experiments was much narrower, which means less cutting force would be applied at each instance. Thrust forces were higher than Shamoto and Moriwaki's result because

the vertical speed of the tool was not increasing as fast as Shamoto and Moriwaki's experiments due to the low ratio of depth of cut per vertical vibration amplitude.

Cerniway modeled the elliptical vibration machining motion in relation to the chip thickness. In the orthogonal cutting, the chip thickness is equal to the total depth of cut, but it is reduced to the thickness of the shaded area as shown in Figure 2.3. Thus the forces required for chip removal is reduced compared to the conventional orthogonal cutting.

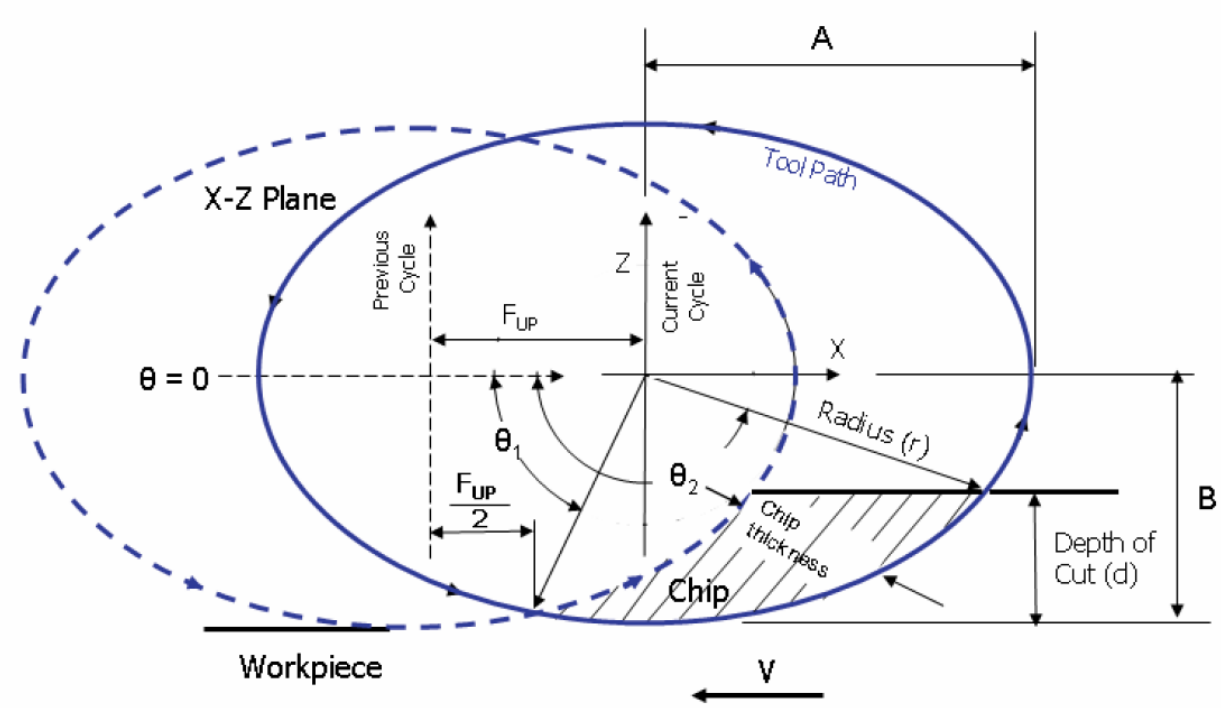

Figure 2.3 Model of Elliptical Vibration Machining in relation to chip thickness [Cerniway 2001]

Several experiments on elliptical vibration machining are introduced to show the benefits of the method in tool wear, surface finish and choice of materials. Shamoto and Moriwaki performed turning experiments on hardened steel with elliptical vibration machining [Shamoto and Moriwaki, 1999]. The tool used in this experiment was a polycrystalline diamond (PCD) tool with the nose radius of 1 mm. Over the long period of experiments, tools used in conventional 1-D vibration assisted machining experienced rapid increase in forces and had to be stopped at

1000 m of cutting distance. At the same time, tools used in elliptical vibration machining experienced gradual increase in cutting forces up to cutting distance of 3000 m as shown in Figure 2.4.

The rapid increase of cutting forces in 1-D vibration assisted machining is due to the diamond tools being chipped away while diamond tools used in elliptical vibration machining was gradually worn out with even geometry. Similar results were reported by Cerniway as well. He compared the tool from conventional orthogonal turning of steel with diamond tool and elliptical vibration machining of steel with diamond tool. The scanning electron microscopy (SEM) images of tools reveal that conventional orthogonal machining left triangle shaped grooves worn into tool edges while vibration assisted machining left smooth and continuous curves [Cerniway 2001].

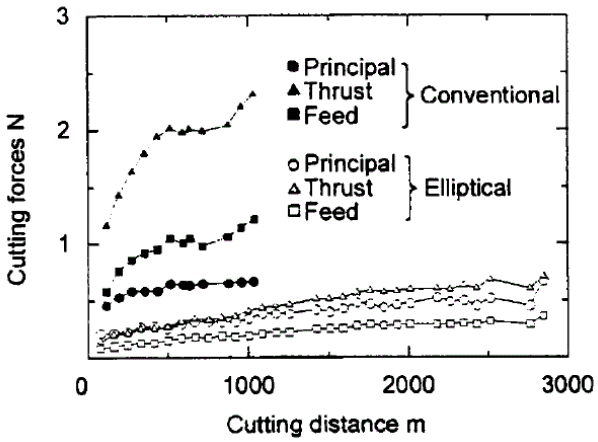

Figure 2.4 Comparison of cutting forces between 1-D and elliptical vibration machining [Shamoto and Moriwaki 1999]

Furthermore, Brinksmeir and Glabe extended the discussion and related the tool wear rate to the effective contact time [Brinksmeir and Glabe 1999]. They used diamond tool with the nose radius of 3 mm against carbon steel, and performed turning experiments at vibration frequency

of 40 kHz and amplitude of 6 μm. They reported that cutting distance decreases as the effective contact time increases. At 22% of effective cutting time (the ratio of time where the tool is in actual contact with the workpiece material in comparison to the overall machining time), they achieved 20 m of cutting distance with precise surface finish, but no wear reduction was found once effective contact time reaches 54 %.

There were more investigations regarding the surface characteristics of the workpiece materials after elliptical vibration machining. Elliptical vibration machining leaves inherent mark on the surface due to its elliptical motion; however, this happens in controlled manner. The surface finish is improved significantly compared to both traditional cutting method and 1-D vibration assisted machining due to the reduction in forces and tool wear, eliminating unnecessary vibrations and maintaining sharp tool.

Shamoto and Moriwaki presented that elliptical vibration machining can achieve better form accuracy. They used a HSS (high speed steel) tool for quasi-orthogonal machining of the OFC (oxygen free copper) workpiece, and achieved better shape accuracy than ordinary cutting method. However, the surface roughness was at 0.02 μm, which was larger than that of the ordinary cutting while still smaller than the surface roughness of the 1-D vibration assisted machining [Shamoto and Moriwaki 1994].

They continued their research onto the machining of steel with diamond tool. They first machined hardened die steel (JIS: SUS420J2) at hardness of HRC39 with a diamond tool. The surface roughness decreased as the feed rate was decreased, but it converged to the value of 0.025 μm, the maximum peak value, at 10 μm/rev of feed rate and was not reduced any further. Thus the most effective feed rate with better surface quality was found to be 10 μm/rev; at this

feed rate, they obtained the optical quality surfaces with maximum roughness of less than 0.05 μm up to a cutting distance of the impressive 2250 m [Shamoto and Moriwaki 1999].

The 1-D vibration assisted machining showed surface roughness 0.04 μm at the cutting distance of 10 m, and the surface roughness reached the value of 0.08 μm already at the cutting distance of 500m, which proves the advantage of the elliptical vibration machining (See Figure 2.5). They applied the elliptical vibrations to turning of a spherical die as well. Hardened die steel (JIS: SUS440C with the hardness of HRC61) was used in this experiment, and this time they obtained 0.02 μm of the peak to valley surface roughness at the cutting distance of 320 m [Shamoto and Moriwaki 1999].

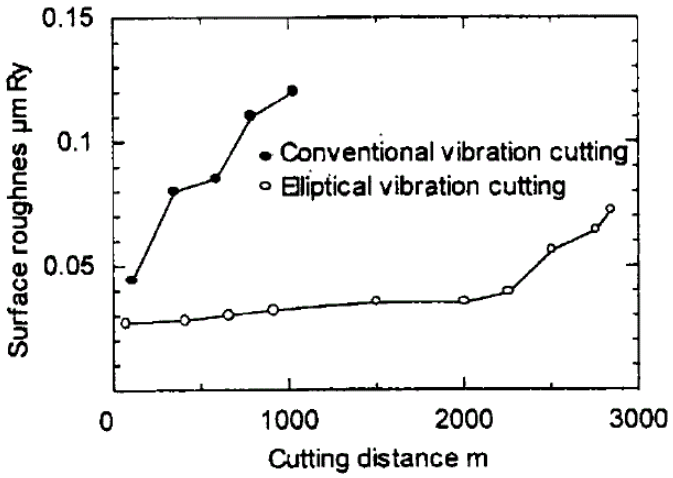

Figure 2.5 Comparison of the surface roughness of the 1-D and elliptical vibration machining [Shamoto and Moriwaki 1999]

Other researchers such as Ahn [Ahn et al. 1999] and Brinksmeir and Glabe [Brinksmeir and Glabe 1999] also reported the improved quality of surface finish through elliptical vibration machining. Ahn et al. machined a brass workpiece with a diamond tool, and observed improved surface finish in elliptical vibration machining compared to the conventional machining without any vibration applied, especially as the cutting speed increased. They also observed that during

conventional machining, the surface roughness was fluctuating due to the unstable cutting mechanism such as the plowing, while the elliptical vibration machining had very stable surface roughness even when the depth of cut was less than 2 μm. They achieved the mean surface roughness r_a of about 0.04 μm, the maximum height of the peak [Ahn et al. 1999].

Brinksmeir and Glabe studied and compared the surface characteristics of elliptical vibration machining in two different materials, namely the aluminium and the carbon steel (0.45% carbon). While aluminium had consistent peak to valley values, carbon steel showed variations in height for one feed mark to the next one, though carbon steel showed less surface roughness. He achieved approximately 0.05 and 0.02 μm of the peak to valley values of surface roughness for aluminium and carbon steel, respectively [Brinksmeir and Glabe 1999].

The more recent study of Nath et al. performed challenging experiments of machining extremely hard material such as the tungsten carbide. They observed that the surface roughness increases as the machining speed ratio increases. They defined the speed ratio as the ratio of the nominal cutting speed to the maximum tool vibration speed in the cutting direction. After machining tungsten carbide for 60 minutes using a polycrystalline diamond tool, they achieved 0.03 to 0.05 μm of average surface roughness [Nath et al. 2009].

The elliptical vibration machining is also known to reduce the formation of burrs. Burr formation reduces the accuracy of the machining process, and the cost of burr removal and the time spent during the process takes a considerable amount of total machining cost and time [Ma et al. 2005]. Through theoretical analysis, they found that the average pushing and bending stress of deformation zone in burr formation is smaller during the elliptical vibration machining compared to the ordinary cutting and the 1-D vibration assisted machining [Ma et al. 2005].

Researchers have reported the suppression of burr formation using the elliptical vibration machining, with and without the knowledge of the theoretical analysis. Ahn and others performed machining experiments on varying depths of cuts on the brass workpiece, and reported that burr started forming at 1 μm depth of cut for non-vibrant ordinary cutting process, but there was hardly any burr formed even at 5 μm depth of cut for elliptical vibration machining process [Ahn et al. 1999].

Ma and others measured the actual height of burrs after ordinary cutting, 1-D vibration assistant machining and the elliptical vibration machining. A carbide tool was used on an aluminum workpiece, and the depth of cut was kept at 50 μm. Ordinary cutting exhibited almost 100 μm of burr formation, while the conventional 1-D vibration assisted machining showed approximately 40 to 20 μm of burr formation. The elliptical vibration machining showed approximately 10 μm of burr formation at the low speed ratio ($SR < 2$), and there was almost no burr formation if the speed ratio was high enough ($SR > 6$) [Ma et al. 2005].

As it was described above, scholars and researchers have studied EVM process and observed that EVM process can reduce forces, tool wear and burr formation, and improve the surface finishes. However, the process is still not fully understood to be able to explain which parameters affect them. Further investigations in the mechanism of EVM process is required to obtain optimal conditions for EVM process.

2.2.2 Current EVM Systems

Mechanical systems for elliptical vibration machining utilize the resonance of system at a natural frequency to amplify the vibration exerted by piezoelectric actuators. There are several designs proposed by other researchers; however, the fundamental of designs are very similar to that of Shamoto and Moriwaki's works. Shamoto and Moriwaki created and updated design

through their development processes [Shamoto and Moriwaki 1994; 1995; 1999], as shown in the Figure 2.6. Two pairs of piezoelectric actuators were attached to the side faces of the beam structure, and they were activated in opposed pairs to induce bending motion.

However, there was a downside to this design. Modal frequencies of the two vibration directions were very close to each other, thus crosstalk occurred. Crosstalk occurs when the energy is being transferred between two modes, and it causes the tool path to be distorted from the desired path. Therefore, Shamoto and Moriwaki developed a feedback control system to compensate for the crosstalk. Piezoelectric strain gauges were attached to the system; their purpose was to measure the displacement of the beam and compensate for the crosstalk by adjusting the input voltage. As a result, the error of shape accuracy was improved from 2.0 μm to 0.2 μm with the dynamic compensation applied.

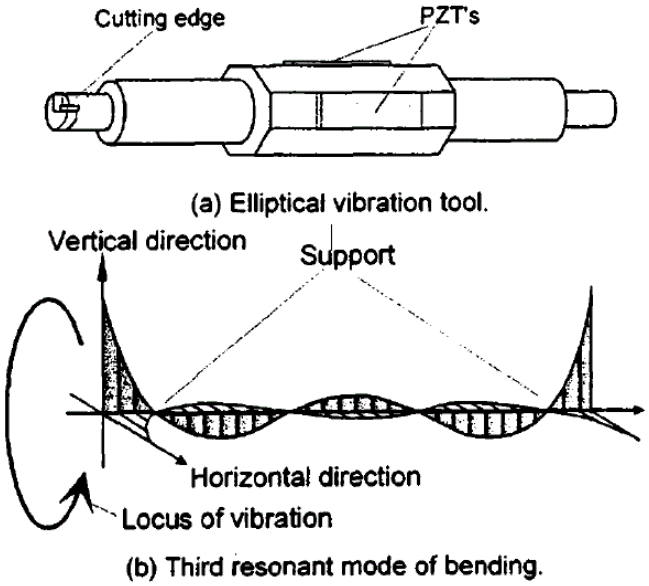

Figure 2.6 A resonant EVM system [Shamoto and Moriwaki 1999]

Not all elliptical vibration machining systems work at the resonant frequency. Cerniway developed a non-resonant elliptical vibration machining system, as shown in Figure 2.7. In this

system, two parallel actuators are connected to a mechanical linkage. By exciting two actuators at different phases, linear motion of actuators would be converted into elliptical motion. Unlike the resonant elliptical vibration machining system proposed above, this type of system is able to operate over a varying range of frequencies. It is also easier to control the aspect ratio, orientation and tool path size by manipulating the amplitude and phase of two actuators [Cerniway 2001]. However, the system involves more parts and moving joints. Under continuous exposure to high frequency vibration, heat accumulation and material fatigue could be limiting factors to this kind of systems.

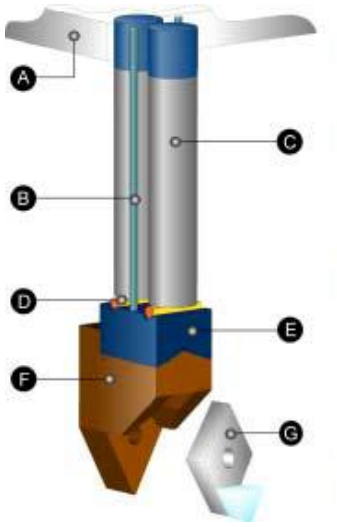

Figure 2.7 Non-resonant EVM system [Cerniway 2001]

As it was presented above, there are various experimental studies on how EVM improves machining efficiency, but there are only very few studies explaining the reason. Even their studies require further investigations to understand it better. Therefore, it is required to design and build an experimental EVM system with more flexibility, free of disadvantages shown in resonant and non-resonant EVM systems shown here.

2.3 Chapter Summary

With the understanding of superior material properties of CNTs, it was described how polymeric CNT nanocomposites are enhanced with the addition of CNTs and how their properties can be controlled by altering CNT alignments and dispersion. However, there were very few studies on the mechanical machining characteristics of polymeric CNT nanocomposites with aligned CNTs, and even the existing ones were limited to either the finite element simulations or just micro milling techniques. In order to obtain more fundamental understanding of micro mechanical machining of polymeric CNT nanocomposites with CNT alignments, it is required to study the micro scribing as suggested in this study.

Demands for more advanced micro mechanical machining techniques were addressed by the development of elliptical vibration machining technique as it can significantly reduce applied forces during the process. In this chapter, literature describing the fundamentals of EVM techniques and their effects in force reduction were introduced. Mechanics of EVM process is still not understood fully, existing theories have limitations that they fit specific experimental conditions; a more general force model is required. However, current EVM systems are either limited in operational range of motion or vibration frequencies, which requires the development of a more flexible and versatile EVM system.

CHAPTER 3. INVESTIGATION OF MICRO SCRIBING OF MWCNT-PS COMPOSITES

The mechanics of micro scribing of polymeric CNT nanocomposites are examined by investigating the relationship of material properties obtained from micro indentation and forces from micro scribing process. Experiments were performed on the MWCNT-PS nanocomposite samples with partial alignment, prepared through the micro injection molding process. A micro indenter-scriber system capable of continuous measurement of applied forces during the scribing and indentation process was developed in-house.

Using the developed system, scribing tests were performed in two different directions – parallel (in-flow) and perpendicular (cross-flow) to the CNT alignment. The ratio between the horizontal cutting and vertical thrust forces (i.e. apparent friction) were analyzed. Indentation tests were performed at five different indentation depths, measuring forces in corresponding indentation depths at each CNT concentration. The results were qualitatively analyzed, and a novel force model was proposed to explain the relationship between material properties and scribing forces quantitatively.

3.1 Development of Micro Indenter-Scriber System

Micro indentation and scribing processes are similar processes as they both require continuous measurement of forces resulting from deformation of materials due to the tool displacement. They are different only in direction, as indentation requires vertical displacements

of the tool while the scribing requires horizontal displacements. It is possible to have a combinatory system to perform both micro indentation and scribing experiments in one system, using the same tool. Thus, an experimental indenter-scriber system was developed, allowing 3 axial displacement and force measurements.

The indenter-scriber system consists of several components as depicted in Figure 3.1: a nano-positioning stage, sensors, structural support with the rigid indenter probe, and a data acquisition system. A single crystal diamond Berkovich tip is used in the scratching and indentation tests. Unlike atomic force microscopes (AFMs), which require relatively lengthy calibration procedures and are limited in their maximum force due to cantilever stiffness [Sader et al. 1999], the new system has a rigidly attached diamond probe to exert sufficient forces.

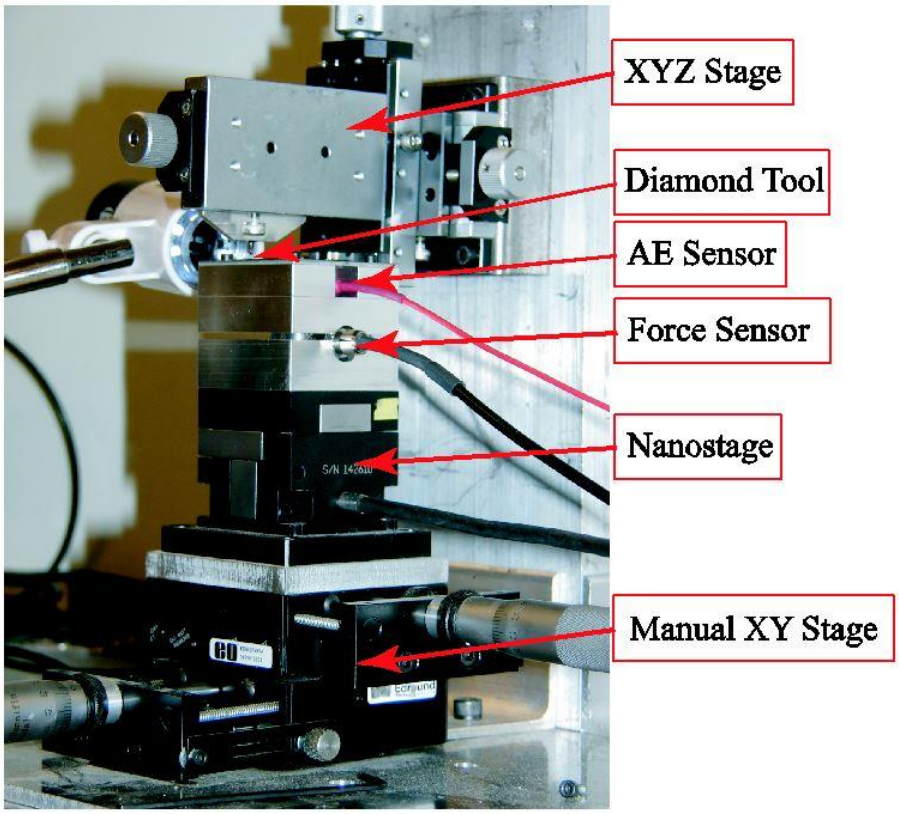

Figure 3.1 Pictorial view of the micro indenter-scriber system

To prevent any damage to the system and to avoid noise, the whole system is mounted on top of a vibration isolating table. In order to guarantee the accuracy of the measurement, it is important to calibrate the sensors and identify disturbances during the measurement. In this section, the instrumental compliance of the system is identified, and the calibration of nanopositioning stages and sensors is also presented.

3.1.1 Nanopositioning Stage

The core of the displacement control system is the piezoelectric stage (PI NanoCube P-611.3S), combined with its controller (PI E664). The piezoelectric stage is capable of making displacement in the range of 100 μm in 3 axes, with the resolution of 1 nm at closed-loop circuit. It can apply force up to 15 N. The piezoelectric stage has integrated strain gauge sensor, recording actual displacement made by the piezoelectric stage through the data acquisition system provided. The piezo-stage has minimal thermal drift in the closed loop mode by compensating through the sensors.

The piezoelectric nanopositioning stage is calibrated for accurate displacement control. The same capacitance is installed on top of the piezoelectric stage, and the continuous displacement signals in manners of the step and the ramp are applied. The relationships between the measurements of the capacitance sensor, the input voltage and the internal strain gauge inside the piezoelectric stage are plotted and compared. As the result, a ratio of 9.397 μm/V for cap sensor/strain gauge, and a ratio of 9.430 μm/V for displacement/input voltage were obtained.

However, the displacement measured in nanostage can be affected by the instrument compliance. The instrument compliance is the displacement error measured as the instrument itself deforms under the load. When indentations are made in materials with a high modulus of elasticity, the instrument compliance might affect the displacement measurement significantly.

Oliver and Pharr suggested that the ratio of total measured displacement over applied load is the sum of the instrumental compliance and the compliance of the indenter material [Oliver and Pharr 1992]. Though, Oliver and Pharr acknowledged that this method is cumbersome and difficult to implement sometimes, and suggested refined calibration method called the continuous stiffness measurement using fused silica [Oliver and Pharr 2004]. However, this method also requires repetitive indentations of reference material, such as the fused silica.

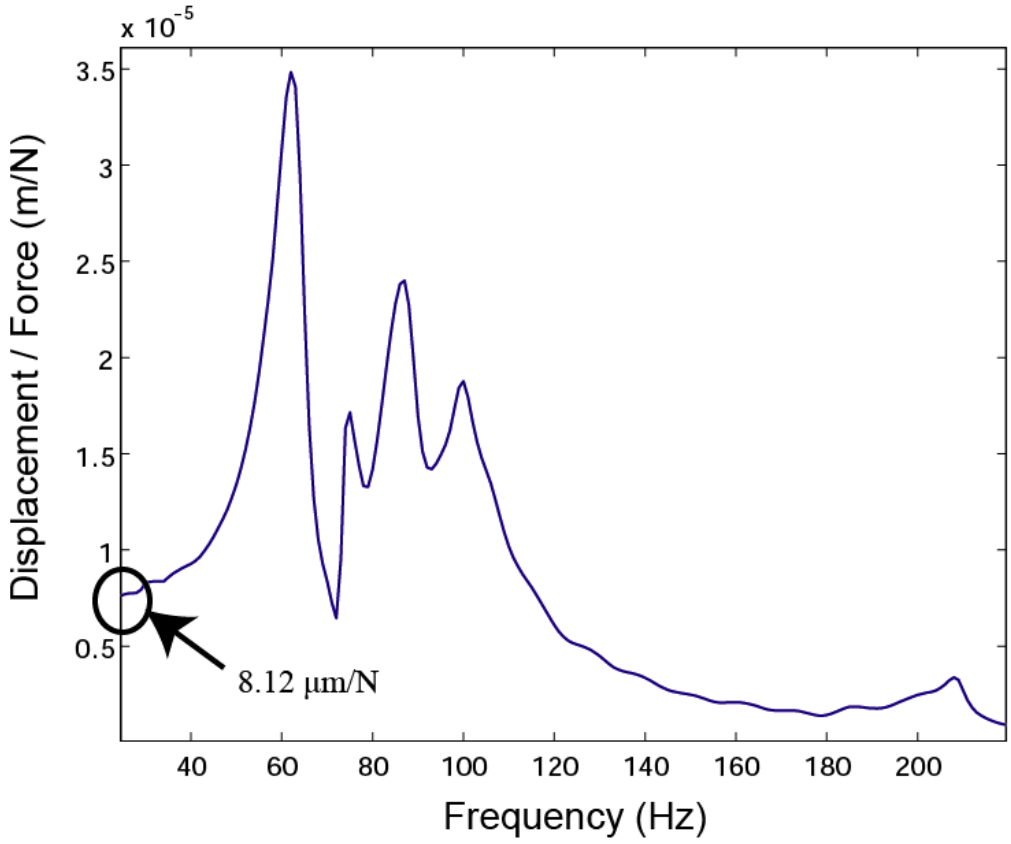

Figure 3.2 FRF of Micro Indenter-Scriber System under Vertical Impact

The modal analysis technique is used to determine the ratio of the instrumental compliance to the applied force. An impact hammer (PCB 208 A03) applies vertical impact force to the tool holder and the displacement response is measured using the capacitance sensor (Lion

Precision DMT20). Cutpro^{TM} 9.0 is used to analyze the frequency response function, and plotted the ratio of displacement to the force versus the frequency (Figure 3.2). This is the technique often used for dynamic analysis, though it can be applied to the case with the static load. The value at the zero frequency level is the ratio of instrumental compliance to the force at the static loading. Displacement data from experiment will be compensated using this ratio in accordance with the force measurement.

3.1.2 Sensors

The force sensor (Kistler 9017B) used in this system can sense three axis of forces. In the z-axis, it has maximum 2 kN of force capacity with sensitivity of 11 pC/N. Signals from the force sensor are amplified by dual mode charge amplifiers (Kistler 5010). Two plates, each called top force plate and bottom force plate, encase the force sensor between them. The bottom force plate sits on top of the piezoelectric stage, and the top force plate is connected to the acoustic emission sensor casing. The acoustic emission (AE) sensor (Physical Acoustics Nano 30) is attached at the bottom of the sample plates. The AE sensor can identify the point of contact to set up the datum point.

For the force sensor calibration, the transducer sensitivity of the charge amplifier was adjusted instead of the obtaining calibration factor for post analysis. The same impact hammer that was used in the instrument compliance measurement is utilized again for the force sensor calibration. It goes through iterative process until the ratio of measured force from the force sensor and the hammer is close to 1 with less than 1 % error (i.e. DC component). The transducer sensitivity values obtained for the *x*, *y* and *z* directions are 3.99 mV/N, 4.27 mV/N, and 10.0 mV/N, respectively. Moreover, the noise floor level (i.e. amount of noise at presence before the force is applied) is found to be approximately 13% of the force measurements. The data

acquisition system (NI SCXI 1302 and NI SCXI s1305) combined together with a personal computer is controlled by a custom-built code (NI Labview^{TM}).

3.1.3 Diamond tool

A Berkovich-shaped single crystal diamond probe is used, as illustrated in Figure 3.3. The tip radius was identified by scanning electron microscopy (SEM) and analyzed with the ImageJ^{TM} software. It was determined that the tip has a radius, *r*, of 0.88 μm. The probe is rigidly attached to the three-axis manual positioning system which allows coarse adjustment of the tool position.

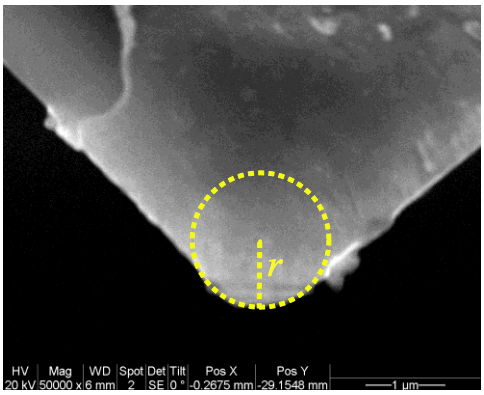

Figure 3.3 SEM image of the diamond probe (Front view)

The Z-axis tool setting is another important aspect for the accurate measurement of depth. The tool approaches the workpiece surface using a coarse manual positioning system, while the tip is monitored using a digital microscope (Digitex 200) at 200x magnification during the process. The fine adjustment is then made by approaching the nano-stage using the piezoelectric controller until a signal is observed from the force and AE sensors.

3.2 Preparation of MWCNT-PS Nanocomposites

In this study, MWCNT-PS mixtures are used to investigate the behaviour of polymeric CNT nanocomposites under mechanical deformation, namely the indentation and scribing experiments. The samples, with dimensions of 25 mm by 10 mm and a thickness of 0.7 mm, are prepared using a micro injection molding machine (Boy 12A). The CNTs are partially aligned in the polymer matrix due to shear stress applied by high pressure melt flow.

It is advantageous that the micro injection molding technique does not require any additional equipment to induce CNT alignment, and it is relatively easy to prepare samples with different CNT concentrations. The MWCNT-PS pellets (Hyperion Catalysis) are diluted with pristine PS (Americas Styrenics Styron 610) using a twin-screw extruder. A total of four different samples with varying MWCNT loadings are prepared: 0.0, 0.5, 2.0 and 5.0 wt.%. During the injection molding procedure, the injection/holding pressure is kept at constant 10 MPa while the injection speed and melt temperature are set to 240 mm/sec and 215 ℃, respectively. Both the holding and cooling times are set to 8 seconds each.

Figure 3.4 shows a transmission electron microscopy (TEM) picture of a prepared sample that indicates the direction of the CNT alignment, which follows the melt flow direction. Some degree of agglomeration can be observed as well. Prepared samples are then used for the micro indentation and scribing forces.

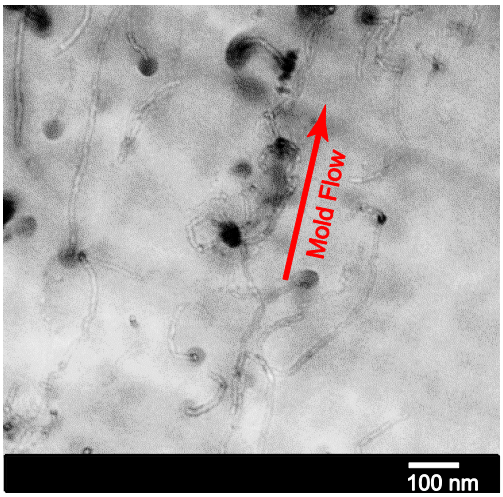

Figure 3.4 TEM image of 2 wt.% MWCNT-PS sample

3.3 Comparative Analysis of Micro Scribing Forces

Force signals measured during the scribing experiments are direct observation of how the material would behave under forces to fabricate features by mechanical means. Scribing tests are performed in two different directions – parallel (in-flow) and perpendicular (cross-flow) to the CNT alignment at each different concentration of CNTs. In this section, forces measured during the scribing experiments and the ratio between the horizontal cutting and vertical thrust forces (i.e. apparent friction) are examined and compared to each other.

3.3.1 Micro Scribing Experimental Procedures

Scribing experiments were performed on samples with three different CNT concentrations. First, the pristine polystyrene sample was tested, and then the MWCNT-PS nanocomposite samples with 0.5 and 5 wt.% of the CNT loadings. Scribing was performed in the in-flow (parallel to the CNT alignment) and cross-flow (perpendicular to the CNT alignment) directions for each sample by alternating the sample placement, with a depth of cut of 5.0 μm and a feed rate of 1.0 μm/s. The orientations of CNT and feed directions are shown in Figure 3.5.

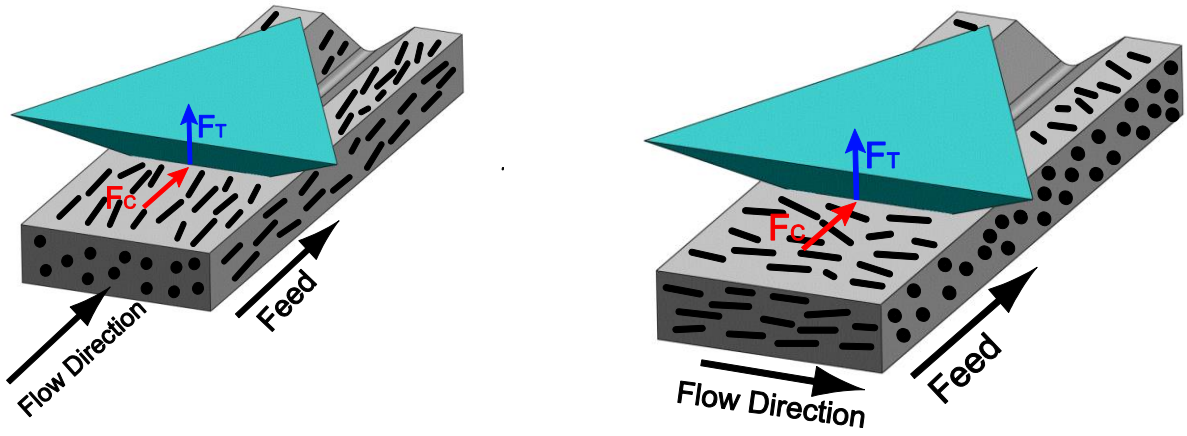

(a) In-flow scribing (b) Cross-flow scribing

Figure 3.5 Scribing experiments with respect to the CNT alignment

The tool was oriented in a way that the face of the tool is fed into the scribing material, not the edge. The primary cutting forces (F_C) are measured in the lateral direction, along the feed direction whereas the thrust forces (F_T) are measured in the axial direction, vertically perpendicular to the feed direction.

All experiments were repeated five times in order to obtain repeatability. Cutting and thrust forces measured in scribing experiments, along with the ratio of these two forces, were comparatively analyzed at different CNT concentrations. Results are discussed with respect to the effects of scribing orientations.

3.3.2 Micro Scribing Force Measurements

Cutting and thrust forces measured from the three axis force sensor were analyzed for each scribing conditions, as depicted in Figure 3.6. It was observed that if the feed rates and the cutting depths were kept constant, varying CNT concentrations affect the average forces of the MWCNT-PS especially the thrust forces. The thrust forces measured from scribing 0.5 wt.%

MWCNT-PS were the highest compared to the pure and 5 wt.% CNT composites. The higher hardness for 0.5 wt.% MWCNT-PS was also observed during indentation experiments. It was hypothesized that adding a small amount (i.e. 0.5 wt.%) of CNTs can make the material harder whereas adding a higher amount (i.e. 5 wt.%) of CNTs would make the material less ductile, resulting in smaller forces in the thrust direction due to crack propagations. It has been reported by others that an increased concentration of CNT in the polymer matrices created stress concentrations due to agglomeration of CNTs at the interface between the polymer and CNTs, resulting in cracks propagating more easily [Samuel et al. 2009].

Results of the in-flow (parallel to the CNT flow) and cross-flow (perpendicular to the CNT flow) scribing of MWCNT-PS nanocomposites were compared. Scribing in the cross-flow direction resulted slightly higher forces than scribing in the in-flow direction for 5 wt.% MWCNT-PS samples.

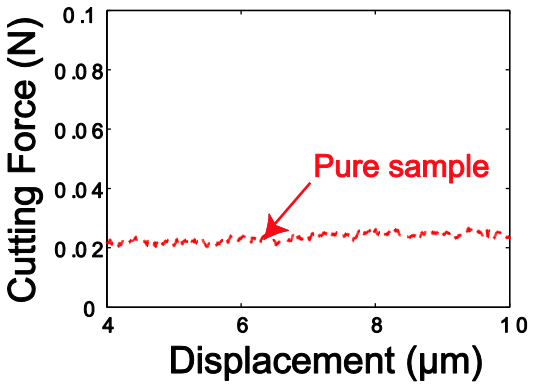

(a) F_C of pure PS

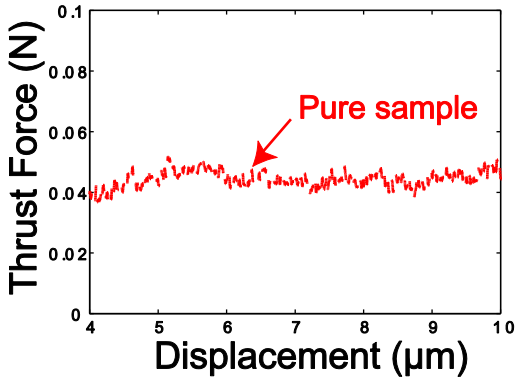

(b) F_T of pure PS

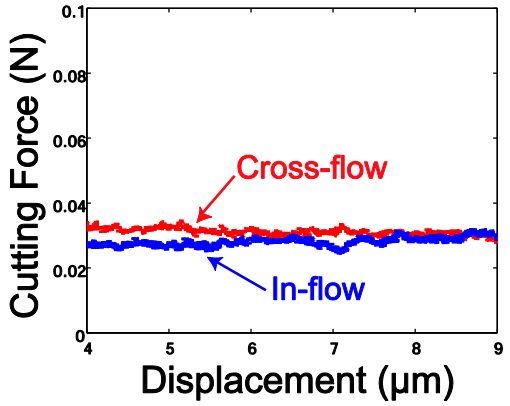

(c) F_C of 0.5 wt.% MWCNT-PS

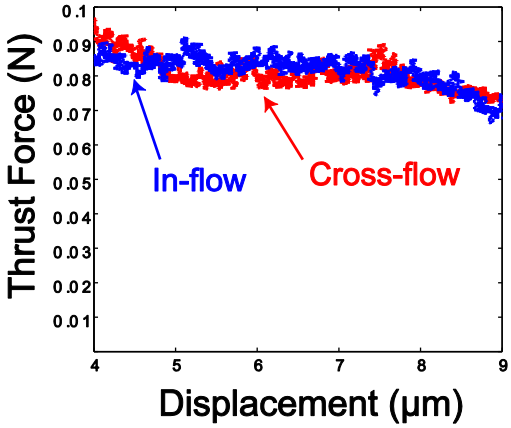

(d) F_T of 0.5 wt.% MWCNT-PS

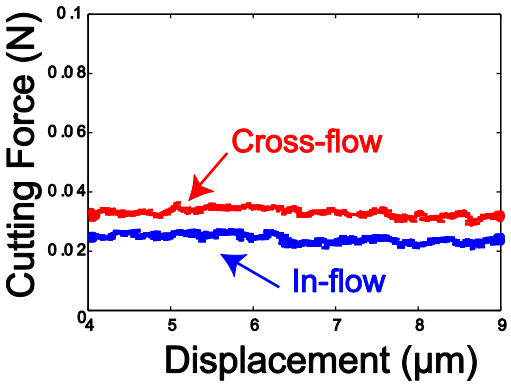

(e) F_C of 5.0 wt.% MWCNT-PS

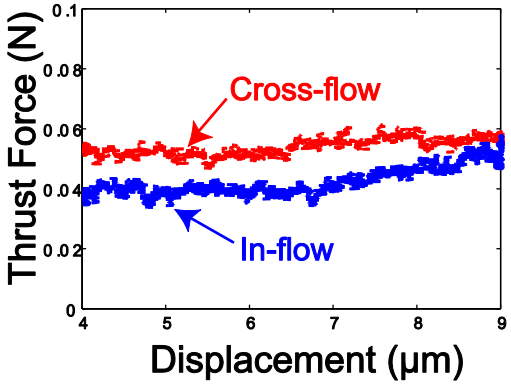

(f) F_T of 5.0 wt.% MWCNT-PS

Figure 3.6 Forces of MWCNT-PS scribing in varying CNT concentrations and orientations

When the cutting is in the in-flow direction, ends of CNTs may act as stress concentrators causing crack formations at lower strains and resulting in lower forces. In the case of scribing in the cross-flow direction, the higher forces are observed as the diamond probe interacts more with CNTs. CNTs may be bent and eventually breaks in the in-flow direction. The difference in forces caused by CNT alignment was more distinctive in samples with higher CNT concentrations. Whereas for small CNT loading (0.5 wt.%), the CNT orientation did not significantly affect the forces.

The apparent friction coefficients (F_C/F_T) between pure, 0.5 and 5 wt.% CNTs were also compared. The results are depicted in Figure 3.7. In general, the apparent friction coefficient

decreased while scribing in the flow direction compared to the cross-flow direction for the CNT nanocomposites. The apparent friction coefficients on varying concentrations of CNT were also investigated, and 0.5 wt.% CNT samples showed the lowest apparent friction coefficient in comparison to the other samples. The conclusion is that a small amount of well dispersed CNTs may decrease the friction coefficient by acting as a dry lubricant. Yang et al. suggested self-lubrication effect of CNTs as a mechanism to improve the wear performance of CNT polymer nanocomposites [Yang et al. 2005]. With increased hardness, the tool slides over the surface more easily. However at higher CNT concentrations, CNTs may act as abrasives rather than lubricants, resulting in higher apparent friction coefficients.

The cutting and thrust scribing forces in varying CNT concentrations and orientations have been investigated. It has been found that addition of small amount of CNTs would increase the scribing forces and further addition of CNTs decrease the forces due to the poor dispersion and agglomeration, resulting in easier crack propagation.

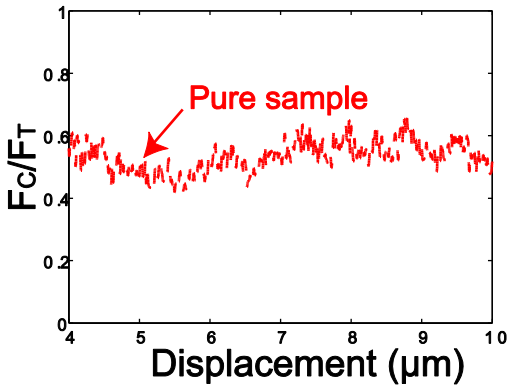

(a) F_C/F_T of pure PS

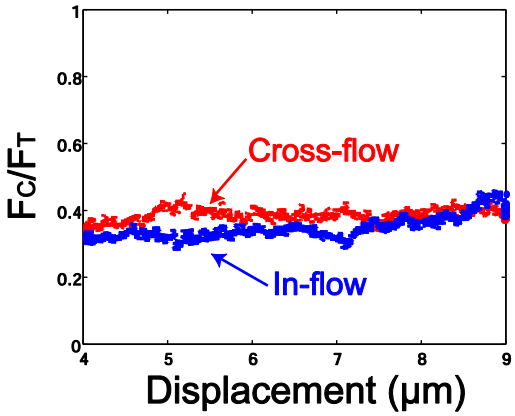

(b) F_C/F_T of 0.5 wt.% MWCNT-PS

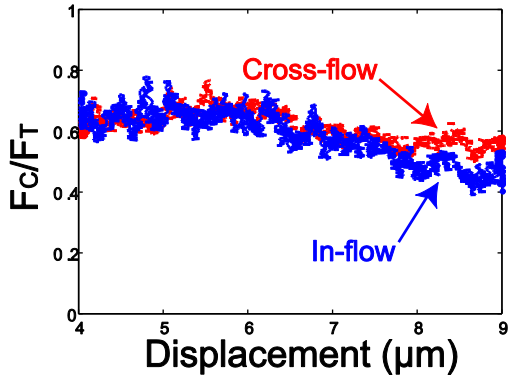

(c) F_C/F_T of 5.0 wt.% MWCNT-PS

Figure 3.7 F_C/F_T of MWCNT-PS in varying CNT concentrations and orientations

The difference in scribing forces due to the CNT orientation can be observed more clearly at higher CNT concentration. Though the dispersion might be poor, alignment is still maintained. Behaviour of the scribing forces found in this experiment can be described in relation to the material properties found from the indentation results, which is presented in the next section.

3.3 Comparative Analysis of Micro Indentation Results

Micro-indentation experiments were performed to identify the material properties, namely the hardness and the modulus of elasticity. These properties are important, not only because they are used to identify the pileup height during the scribing process, but they also have a strong relationship to the scribing parameters.

The analytical indentation procedures used in this study were based on Oliver and Pharr's method [Oliver and Pharr 1992], utilizing the unloading curves from the force-displacement plot. Each unloading curve was fitted to the power law relation of equation (3.1), in order to extract the power law fitting constants, a_p and m:

$$F = a_p (h - h_p)^m \tag{3.1}$$

The difference between the indentation depth, h, and the plastically deformed depth after indentation, h_p, represents the displacement during the unloading step. The plastically deformed depth, h_p, can be measured by finding the x-intercept of the force unloading curve. Figure 3.8 illustrates the sample force unloading curve from indentation of pure PS. The slope of the unloading curve, dF/dh, at its maximum indentation depth, h, is derived from the tangent line by differentiating the unloading curve. By fitting the experimental data, we obtained m (varied from 1.74 to 5.54) and a_p (varied from 0.0105 to 0.110).

The indentation hardness, H (GPa), can be extracted from a simple equation of the maximum force, F_{max}, which is the force at the maximum indentation displacement of the unloading curve, over the projected area of indentation, A_p:

$$H = \frac{F_{\max}}{A_p} \tag{3.2}$$

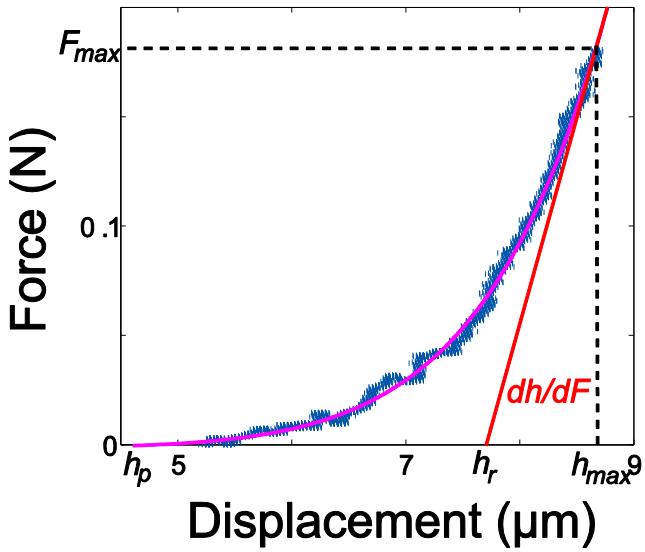

Figure 3.8 Indentation unloading curve of pure PS

In order to find the modulus of elasticity of indentation, E, the reduced modulus of elasticity, E_r, the modulus of elasticity of the indenter, E_i, and Poisson's ratios of the indenter, υ_i, and the sample, υ_s, are required:

$$E = \frac{1-\nu_s^{\,2}}{\frac{1}{E_r} - \frac{(1-\nu_i^{\,2})}{E_i}} \quad \text{where} \quad E_r = \frac{1}{2}\frac{dF}{dh}\frac{\sqrt{\pi}}{\sqrt{A_p}} \tag{3.3}$$

In this study, Poisson's ratio of the diamond indenter, ν_i, was assumed to be 0.07; and, the modulus of elasticity of the indenter, E_i, was assumed to be 1140 GPa as identified by the manufacturer. Poisson's ratio of the composite samples, ν_s, was assumed to be constant at 0.34, which is the same as Poisson's ratio of pure PS. Such an assumption is viable if the amount of MWCNT was low compared to the PS matrix [Kim et al 2009]. Chung et al. also reported that SU-8 polymer reinforced with MWCNT did not show significant changes in Poisson's ratio in comparison to the pure SU-8 sample [Chung et al. 2006].

It is necessary to find the projected area of indentation, A_p, before the desired parameters can be acquired. The projected area of a Berkovich indenter is given by equation (3.4) with angle θ being equal to 65.3° [Fishcer-Cripps 2002].

$$A_p = 3\sqrt{3}h_c^{\,2}\tan^2\theta \tag{3.4}$$

The projected area of indentation, however, cannot be found directly from the depth of indentation, h. Only the portion of the tool surface where contact stress is applied has to be included in the calculation, and the area is evaluated at the contact depth of indentation, h_c. Due to the elastic recovery of the sample, the contact depth, h_c, cannot be accurately measured after indentation. Instead, the elastic model [Oliver and Pharr 2004] was applied as shown in equation (3.5):

$$h_c = h - \varepsilon(h - h_r) \tag{3.5}$$

The value of h_r is given by the intercept of the tangent line of the unloading curve and the displacement axis, as shown in Figure 3.8. We determined the geometric constant ε from m to obtain more accurate results, as shown in equation (3.6) [Pharr and Bolshakov 2002]:

$$\varepsilon = m\left[1 - \frac{2\Gamma\left(\frac{m}{2(m-1)}\right)}{\sqrt{\pi}\,\Gamma\left(\frac{1}{2(m-1)}\right)}(m-1)\right] \tag{3.6}$$

where Γ stands for the mathematical gamma function. The projected area of indentation for each indentation cycle is calculated using equations from (3.4) to (3.6). Based on these analytical steps, the hardness and the modulus of elasticity can be derived.

Figure 3.9 illustrates the hardness of MWCNT-PS samples at varying CNT concentrations, obtained using equation (3.2). Samples with CNT loads of 0.5 wt.% exhibited a higher value of hardness than pure PS. However, hardness decreased as the CNT concentration increased over

2.0 wt.%. Yang et al. observed a similar trend when they measured the micro hardness of CNT-PS nanocomposites with varying CNT concentrations [Yang et al. 2005]. Such results show similar trend to that of the scribing forces observed above, where small addition of CNT contributes in improving the hardness of the composite but more addition of CNT would cause agglomeration of CNTs, resulting in the decreased hardness.

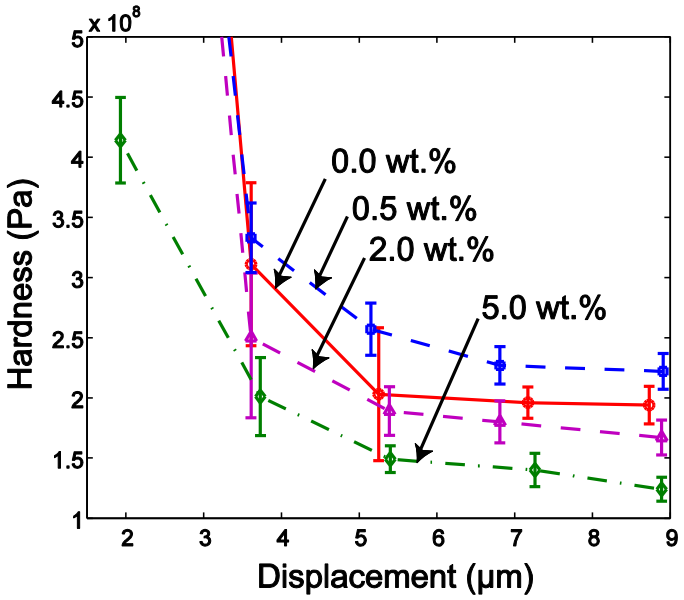

Figure 3.9 Hardness versus indentation depth at varying concentrations of CNT (wt.%)

Figure 3.10 illustrates the modulus of elasticity from equation (3.3). The moduli of elasticity from indentation were very close to each other even at different CNT concentrations, and there was no specific trend observed in relation to the CNT concentration.

The hardness and modulus of elasticity values of pure PS were found to be comparable to the values reported in other literature. The average hardness of pure PS ranged from 0.194 to 0.309 GPa, and the modulus of elasticity ranged from 3.49 to 3.82 GPa depending on the depth of the indentations. The values obtained from indentation experiments for pure PS fell within the

reasonable range from values reported by others with small error [Miyake et al. 2006], as well as the tensile modulus of elasticity of 3.1 GPa provided by the manufacturer (American Styrenics).

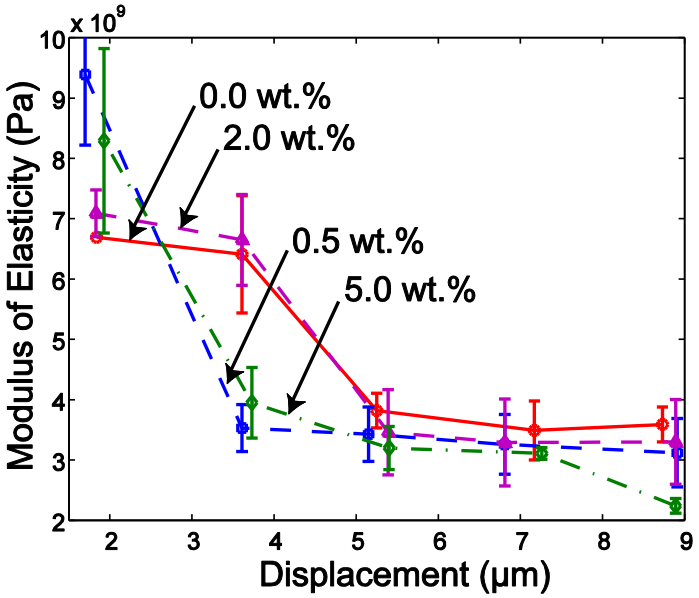

Figure 3.10 Modulus of elasticity vs. indentation depth at varying concentrations of CNT (wt.%)

Errors of the indentation experiments are usually from the inaccurate assumption of the contact area, but the existence of a strain gradient is also known to cause indentation size effects contributing to variance in hardness with respect to the indentation depth. It was assumed that the local flow stress was dependent on the strain, strain rate and temperature; however, strain gradients also existed in the indentation stress field. At a smaller depth of indentation, relatively large strain gradient occurs. Nucleation of dislocations within the plastic zone increases the effective yield strength of the material and increases the hardness as a result [Nix and Gao 1998]. Other than crystalline metals, an amorphous polymer can also experience similar effects due to the kink of polymer chains [Lam and Chong 1999]. Increase in indentation hardness with

decreased indentation size has been also observed with other polymeric CNT nanocomposites [Chung et al. 2006 and Yang et al. 2005].

The modulus of elasticity and hardness of MWCNT-PS, with respect to the CNT concentration, were found from the indentation experiments. The ratio of the modulus of elasticity over the hardness was used to find the maximum pileup height in the scribing force model. In addition, their relation to the scribing forces were identified using proposed scribing force model, which would later be used to estimate scribing forces just from the indentation experiments.

3.4 Micro Scribing Force Modeling

Micro scribing and indentation results provide valuable information regarding their characteristics in mechanical machining processes; however, the mechanism behind the resulting data is still not fully understood. Understanding the mechanism behind the micro-scribing process is important in the prediction of the forces and optimization of the machining processes. A novel micro-scribing force model is proposed to describe measured scribing forces in an effort to fill the gap of knowledge, thus enabling the scribing and indentation data for more practical uses. The forces are described in terms of tool geometry, depth of cut, material properties obtained during indentation experiments, and finally three unknown parameters, representing the coefficients of material removal, material deformation, and friction between the tool and the sample.

Malekian previously investigated in scribing force model of scribing chromium [Malekian et al. 2010]. However, the previous study was in the realm of nano-mechanical machining, where the depth of cut was comparable to the edge radius. It was assumed to be a plowing-dominant

process, where the material flows around the tool edge instead of being removed. Micro-mechanical scribing at a depth of cut higher than the edge radius is not a plowing-dominant process: there is material flowing upward instead of under the tool. The material removal process is also different from the chip removal process usually observed in orthogonal machining, due to the specific tool geometry of a Berkovich indenter, where the highly negative rake angle suppresses chip flows.

When the material is fed into the tool rake face, the material may deform elastically and plastically, flowing under the tool. Any elastic deformation would be recovered once the tool passes. However, if the depth of cut is higher than the stagnation point, some material may flow upward following the rake face through the material removal process. If the depth of cut (i.e., uncut chip thickness) is larger than the height of the stagnation point, the material is translated from the plowing-dominant regime to the shearing-dominant regime, where material deforms and flows around the tool rather than being removed as a chip. The depth of cut exactly at the stagnation point is called the minimum uncut chip thickness, h_m. Malekian and others investigated a method to identify h_m using the minimum energy principle [Malekian et al. 2012]; and, the ratio of h_m over h was found to be 0.226 times the radius, r, for the MWCNT-PS nanocomposites used in this experiment.

There are, therefore, two different material flows at the tool rake face. Materials above the minimum uncut chip thickness flow upward, and the forces associated with this mechanism are annotated as the shearing forces. They are annotated as (1) in Figure 3.11 with the upward material flow. The material constant defining the stress applied during shearing mechanism is represented by the shearing coefficient κ_s.

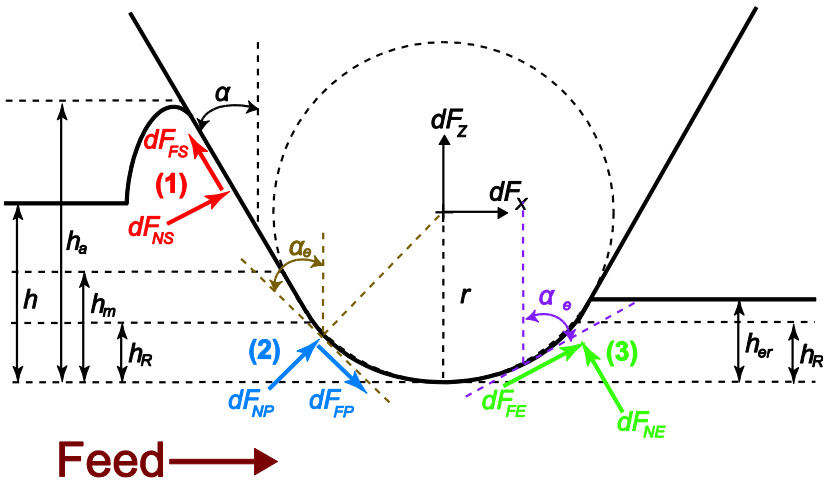

Figure 3.11 Schematic of scribing forces: (1) shearing, (2) plowing and (3) elastic recovery

Materials below the minimum uncut chip thickness flow downward, and the forces associated with this mechanism are annotated as the plowing forces. They are annotated as (2) in Figure 3.11 with the downward material flow around the tool edge. The material constant defining the stress applied to plowing mechanism is represented by the plowing coefficient κ_p.

At the flank face of the tool, certain portion of materials that flowed under the tool though the plowing process would have been recovered elastically, and the forces applied by them on the flank face are annotated as the elastic forces. They are annotated as (3) in Figure 3.11, governed by the plowing process.

Friction between the material flow and the tool surface would be governed by the amount of the normal stress applied on the surface and the adhesion friction coefficient μ_a. While the forces, indentation hardness, modulus of elasticity, tool geometries and elastic recovery ratios are all identified though experiments and observations, these three unknown parameters, κ_s, κ_p and μ_a has to be calculated from the experimental results. In order to identify three unknown variables, three equations are required – therefore, three axes of forces are required.

Scribing processes using a Berkovich diamond tool are generally performed with face-

leading or edge-leading orientation. In these cases, due to their symmetrical geometry, there are only two resulting forces: the horizontal force in parallel to the feed direction and the vertical force orthogonal to the feed direction, as studied in the previous experiments (section 3.2). In this section, scribing experiments were performed with the rake face arranged in asymmetric orientation in order to provide three axes of force measurements.

The feed direction was rotated about the vertical axis of the tool, such that the angle between the feed vector and the normal vector of the tool rake face have an angle of η_c. The angle η_c was determined to be 30 degrees , as shown in Figure 3.12.

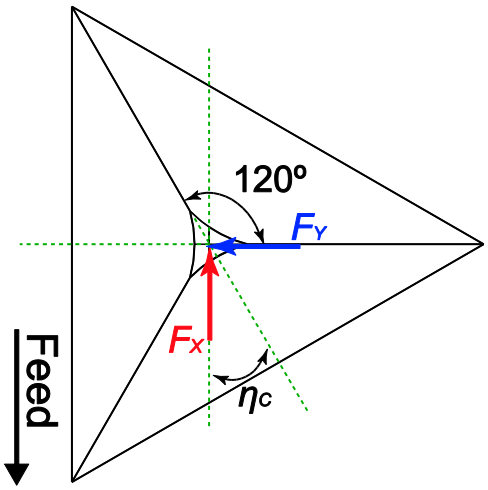

Figure 3.12 Schematic of scribing directions in relation to the tool geometry

The horizontal scribing force, typically known as the cutting force, F_C, was divided into two force components, namely F_X and F_Y. The x-axis force F_X was measured parallel to the feed direction, and the y-axis force F_Y was the horizontal force measured perpendicular to the feed direction. The vertical scribing force, known as the thrust force, F_T, was notated as F_Z for consistency.

All forces in the shearing, plowing and elastic recovery zones are combined together to

describe the three axes of forces measured during the micro-scribing process. Therefore the total force expression is presented as:

$$F_X = F_{XS} + F_{XP} + F_{XE}$$
$$F_Y = F_{YS} + F_{YP} + F_{YE} \quad (3.7)$$
$$F_Z = F_{ZS} + F_{ZP} + F_{ZE}$$

Detailed description of the force components is given in following sections. Each force component in the *X*, *Y* and *Z* axes are described in three regimes of shearing, plowing and elastic recovery process.

3.4.1 Shearing Forces

Material flowing above the minimum uncut chip thickness, h_m, accumulates in front of the tool rake face, while some portion of the material flows around the sides of the tool, left as pile-ups. The amount of material accumulation increases over the scribed distance from the beginning of the scribing, but reaches a critical point where the pileup height is constant. Such behaviour is similar to that of a wedge-forming mode, which is a transitional mode between the plowing and cutting mode suggested by Hokkirigawa and Kato [Hokkirigawa and Kato 2003].

Jardret and others performed a series of experiments on a variety of materials, in order to establish a quantified correlation between the material properties and the height of material pileups, h_a [Jardret et al. 1998]. According to their experimental analysis, the ratio of h_a over the depth of cut, *h*, is determined by the ratio of the modulus of elasticity over the hardness, *E/H*, as expressed by the following equation:

$$h_a = h\left(0.41498\ln\left(\frac{E}{H}\right) - 0.14224\right) \quad (3.8)$$

Bucaille et al. also performed a numerical analysis of scratching of the material [Bucaille et al. 2001]. They compared their results with the experimental results obtained by Jardret and others (1998) and verified that Jardret's experimental data was in good agreement with their numerical analysis if the rheological factor, defined as the ratio of the plastic strain over the elastic strain, was smaller than 100. The samples used in this study all has a rheological factor smaller than 100; therefore, it can be assumed that equation (3.8) is applicable in the prediction of the height of pileups, h_a.

Once the maximum height of pileups is identified, forces acting on the rake face between h_a and h_m can be simply described in terms of the average infinitesimal normal forces, dF_{NS}, and the average infinitesimal friction forces, dF_{FS}, as shown in Figure 3.11. The average infinitesimal normal force, dF_{NS}, can be expressed using the shearing coefficient, κ_s, and the infinitesimal area, dA. The average friction force, dF_{FS}, can be expressed using the average adhesion friction coefficient, μ_a, and the average normal force, dF_{NS}:

$$\begin{aligned} dF_{NS} &= \kappa_S dA \\ dF_{FS} &= \mu_a dF_{NS} = \mu_a \kappa_S dA \end{aligned} \tag{3.9}$$

The shearing coefficient, κ_s, represents the normal stress applied to the tool due to the material flow in combination with the ratio of the side flow and other unknown aspects. The infinitesimal area, dA, can be redefined into terms of the infinitesimal height unit, dh, as dA at each height can be estimated from the geometry of a Berkovich tool. The infinitesimal area dA is represented as:

$$dA = \frac{2\sqrt{3}h\tan\alpha}{\cos\alpha}dh \tag{3.10}$$

The combination of normal and friction forces on the rake face can be translated into the

infinitesimal horizontal forces, dF_{XS} and dF_{YS}, and the vertical force, dF_{TS}:

$$dF_{XS} = \cos\eta_C(\cos(\alpha)dF_{NS} - \sin(\alpha)dF_{FS})$$
$$dF_{YS} = \sin\eta_C(\cos(\alpha)dF_{NS} - \sin(\alpha)dF_{FS}) \quad (3.11)$$
$$dF_{ZS} = \cos(\alpha)dF_{FS} + \sin(\alpha)dF_{NS}$$

Thus, by combining the expressions from equation (3.9) to (3.11) and considering the asymmetric geometry, the following forces can be obtained from the maximum height of pileups, h_a, and the minimum uncut chip thickness (MUCT), h_m:

$$F_{XS} = \cos\eta_C 2\sqrt{3}\kappa_s(\tan\alpha - \mu_a\tan^2\alpha)\int_{h_m}^{h_a} h dh$$
$$F_{YS} = \sin\eta_C 2\sqrt{3}\kappa_s(\tan\alpha - \mu_a\tan^2\alpha)\int_{h_m}^{h_a} h dh \quad (3.12)$$
$$F_{ZS} = 2\sqrt{3}\kappa_s(\mu_a\tan\alpha + \tan^2\alpha)\int_{h_m}^{h_a} h dh$$

Force components in three axes are presented describing the forces applied due to the flow of material flowing upward above the MUCT. Each force component was composed of infinitesimal average normal and friction forces applied to the surface area of the diamond tool.

3.4.2 Plowing Forces

The material that flows under the minimum uncut chip thickness can be modeled using the plowing force model similar to the shearing force model; however, two different geometric functions need to be addressed. The surface area between the minimum uncut chip thickness, h_m, and the depth of the tool where the tool edge is blunt, h_R, maintains the geometry equation of shape of the ideal Berkovich indenter. The surface area would have the shape of inclined trapezoid with the rake angle, α, similar to that of the shearing force model. The only difference is that the material flows in the opposite direction from the previous shearing force model. Below

h_R, the normal and friction forces are applied at a partially spherical surface over a changing effective rake angle, α_e.

The modeling of plowing forces under blunt rounded edges has already been investigated by Malekian and others [Malekian et al. 2010]. With this model, the force, F_{YP}, experiences force components only from the plowing force above h_R, since the partially spherical geometry below h_R is symmetrical and will not have any force in y-axis. Thus, the plowing cutting and thrust forces are expressed in the following equations:

$$\begin{aligned} F_{XP} &= \cos\eta_C 2\sqrt{3}\kappa_p(\tan\alpha + \mu_a \tan^2\alpha)\int_{h_R}^{h_m} h dh \\ &+ \kappa_p \int_{-\pi/2}^{\pi/2}\int_0^{h_R} \cos\eta(\cos\alpha_e + \mu_a \sin\alpha_e) dA \\ F_{YP} &= \sin\eta_C 2\sqrt{3}\kappa_p(\tan\alpha + \mu_a \tan^2\alpha)\int_{h_R}^{h_m} h dh \end{aligned} \tag{3.13}$$

$$F_{ZP} = 2\sqrt{3}\kappa_p(\tan^2\alpha - \mu_a \tan\alpha)\int_{h_R}^{h_m} h dh + \kappa_p \int_{-\pi/2}^{\pi/2}\int_0^{h_R} \sin\alpha_e - \mu_a \cos\alpha_e dA$$

where κ_p is the plowing coefficient; and, η is the angle between the feed direction and the normal vector of the rake face, ranging from $\pi/2$ to negative $\pi/2$. The effective rake angle, α_e, can be expressed as:

$$\cos\alpha_e = \frac{\sqrt{2r\ h - h^2}}{r} \tag{3.14}$$

while the approximate area of the infinitesimal element is then expressed as:

$$dA \cong \frac{r^2}{\sqrt{2rh - h^2}} d\eta dh \tag{3.15}$$

Thus equation (3.13), in conjunction with equations (3.14) and (3.15), represents the material flow under minimum uncut chip thickness as a sum of forces applied in two different regimes, each having geometries of the ideal Berkovich and partial sphere. Plowing force in y-

axis, F_{YP}, is composed of forces from the Berkovich regime only, since the partially spherical geometry is symmetrical.

3.4.3 Forces due to Elastic Recovery

When the material undergoes plowing process, some of the materials are plastically deformed while some are recovered elastically. Elastic recovery of material is often negligible in conventional machining; however, elastic recovery has large effects at the micro regime, thus being an essential component of scribing force model. Malekian et al. have used a conical indenter to scratch materials to identify their elastic recovery ratio, ρ_e, and the same methods were used in this study to identify the elastic recovery of materials [Malekian et al. 2009].

The surface profile was measured using a profilometer (Mitutoyo SJ-301) after scratching. The area of the groove at each infinitesimally small length was calculated from the measured profile, and it was compared to the area of the groove that could have been obtained if 100% of the material was removed. The ratio of the measured area over the estimated area is identified as the elastic recovery ratio, ρ_e. The depth of the elastically recovered material, h_{er}, can be calculated by multiplying the elastic recovery ratio directly to the uncut chip thickness, h.

As the concentration of the MWCNT increased, the elastic recovery rate, p_e, decreased. It was observed that pure PS had an elastic recovery ratio of 29.3%, whereas the MWCNT-PS with a CNT concentration of 0.5 wt.% had an elastic recovery ratio of 26.6%. The elastic recovery rate dropped significantly for MWCNT-PS with a CNT concentration of 5.0 wt.%, as it recovered only 9.94%. With the assumption that the stress applied by the elastic recovery of the material is governed by the same plowing coefficient, κ_p, the forces applied by the elastic recovery of the plowed material can be expressed in equation (3.16):

$$F_{XE} = \cos\eta_C 2\sqrt{3}\kappa_p(-\tan\alpha + \mu_a \tan^2\alpha)\int_{h_R}^{h_{er}} h dh + \kappa_p \int_{-\pi/2}^{\pi/2}\int_0^{h_R} \cos\eta(-\cos\ \alpha_e + \mu_a \sin\alpha_e) dA$$

$$F_{YE} = 2\sqrt{3}\kappa_p(-\tan\alpha + \mu_a \tan^2\alpha)\int_{h_R}^{h_{er}} h dh + \sin\eta_C 2\sqrt{3}\kappa_p(\tan\alpha - \mu_a \tan^2\alpha)\int_{h_R}^{h_{er}} h dh \quad (3.16)$$

$$F_{ZE} = 2[2\sqrt{3}\kappa_p(\tan^2\alpha + \mu_a \tan\alpha)\int_{h_R}^{h_{er}} h dh + \kappa_p \int_{-\pi/2}^{\pi/2}\int_0^{h_R} \sin\alpha_e + \mu_a \cos\alpha_e dA\ ]$$

Forces are in a consistent coordinate system that is the same as the shearing and the plowing cases. In this section, shearing, plowing and elastic recovery force components were described in detail, and the sum of the components could express the total measured forces in three directions. This model was then analyzed with the experimental data to provide valuable understanding of the material behaviour under micro-scribing conditions.

3.4.4 Identification of Parameters for Scribing Force Modeling

The force measurements obtained from the scribing experiments and the material properties identified through the indentation experiments were combined and analyzed using the proposed scribing force model. The resulting scribing coefficients, κ_s, κ_p and μ_a, were identified and plotted in Figures 3.13 to 3.15.

As CNT concentration increased, the shearing coefficient, κ_s, increased for the cross-flow oriented scribing, but decreased for the in-flow oriented scribing as shown in Figure 3.13. This can be explained by fact the increased CNT load in the cross-flow scribing made the material more resistant to the scribing action, as the tool had to either cut through or bend CNT fillers. However, in the in-flow scribing, high stress was concentrated at the interface between CNT fillers and polymer matrices; adding more CNT increases the brittleness and thus material shears away more easily.

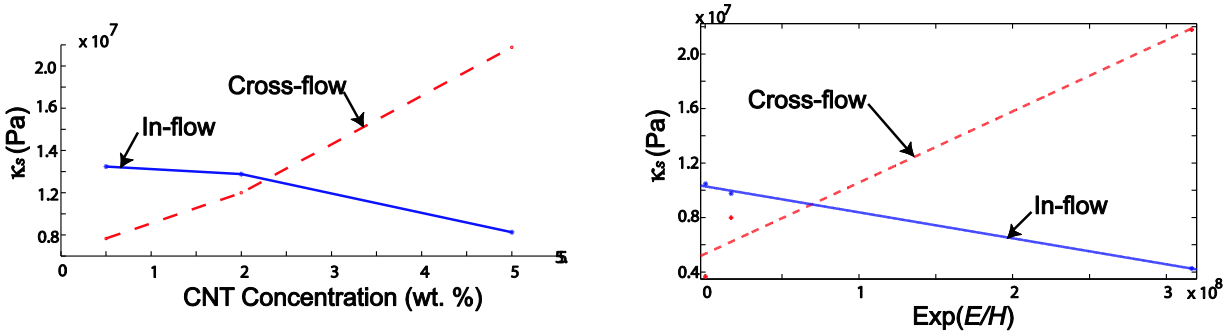

(a) In relation to the CNT concentration (b) In relation to the material properties

Figure 3.13 Shearing coefficient of MWCNT-PS

The plowing coefficient, κ_p, increased with increased CNT loading in both the cross-flow and in-flow orientations as shown in Figure 3.14. In the plowing-dominant region, shearing does not occur; and, the stress concentration would not cause the materials to fail. Therefore, the addition of the CNT only improved the material resistance to scribing. The cross-flow scribing experienced more resistance at higher CNT concentrations, as the in-flow scribing had stress concentration forming at the head or tail of the CNT, allowing for easier crack initiation and propagation.

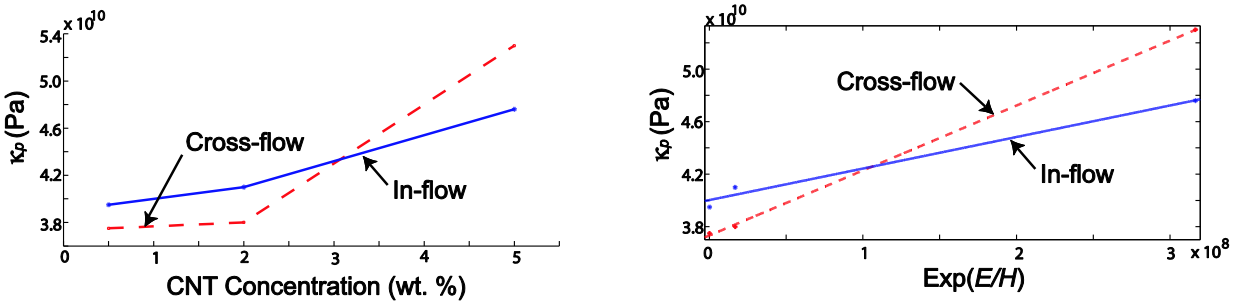

(a) In relation to the CNT concentration (b) In relation to the material properties

Figure 3.14 Plowing coefficient of MWCNT-PS

The adhesion friction coefficient, μ_a, in both orientations decreased with increasing CNT

concentration, but the cross-flow scribing experienced much higher friction coefficients, especially at lower CNT concentrations (see Figure 3.15).

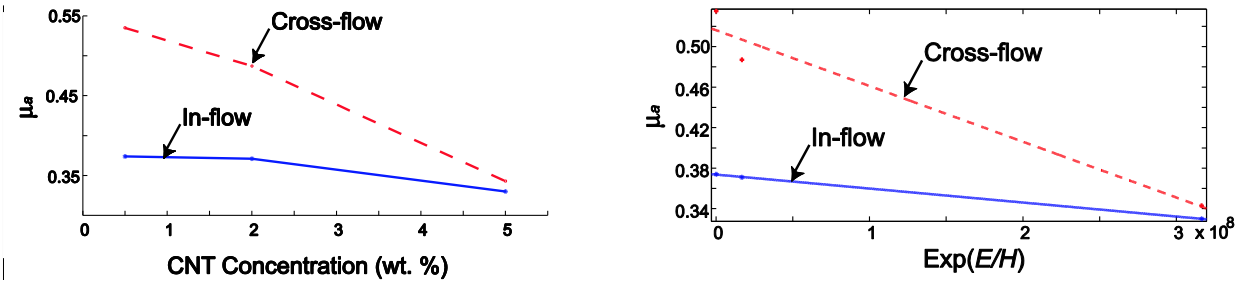

(a) In relation to the CNT concentration (b) In relation to the material properties

Figure 3.15 Adhesion friction coefficient of MWCNT-PS

At higher CNT concentrations, such as 5.0 wt.%, the difference between the cross-flow and in-flow scribing was negligible. One possible explanation may be that, at high CNT concentrations, more CNTs were detached or exposed to the surface, due to the increased brittleness, and acted as a dry lubricant between two surfaces.

These trends can be linearized in relation to the material properties obtained through micro indentations. Graphs of κ_s, κ_p and μ_a were plotted versus the exponential function of ratio of the modulus over the hardness, *E/H*. The linear curve fitting was used, enabling the estimation of scribing parameters as long as the material properties from micro indentation are given, resulting in the ability to predict scribing forces. The relationship between the indentation material properties and the scribing parameters can be represented by a linear polynomial equation as shown in equation (3.17) with the corresponding constants presented in the following Table 3.1:

$$Y = C_1 e^{\frac{E}{H}} + C_2 \tag{3.17}$$

Table 3.1 Constants for linear polynomial relationship between indentation and scribing

Y (Pa)	Scribing Direction	C_1	C_2 (Pa)
κ_s	Cross-flow	5.23E-2	5.33E6
	In-flow	-1.91E-2	6.02E7
κ_p	Cross-flow	4.94E1	3.73E10
	In-flow	2.40E1	4.00E10
μ_a	Cross-flow	-5.50E-10	5.16E1
	In-flow	-1.38E-10	3.73E1

Identified linear polynomial equations can be used to predict scribing forces from indentation experiments only. In order to verify the data obtained, micro indentation and scribing experiments were performed on 0.1 wt.% MWCNT-PS sample. The experimental and simulated scribing forces are presented in Table 3.2.

Table 3.2 Verification of scribing force model

	CNT orientation	Experimental *(N)*	Simulation *(N)*	Error (%)
F_X	Cross-flow	4.13 E-2	4.06 E-2	1.60
	In-flow	3.32 E-2	3.54 E-2	6.22
F_Y	Cross-flow	6.51 E-4	5.93 E-2	9.66
	In-flow	1.14 E-3	1.23 E-3	7.32
F_Z	Cross-flow	6.48 E-2	1.00 E-1	35.3
	In-flow	6.90 E-2	1.11 E-1	37.9

As it is shown in Table 3.2, the horizontal forces F_X and F_Y are within 10% error zone, but the vertical force F_Z has high error percentage. It might be required to have more data points in order to establish more accurate linear polynomial equation for scribing parameters, as well as improvement in the model itself. Currently the model assumes that constant amount of average stress is being applied to the tool surfaces, however, the stress gradient would vary over the depth of the cut. It was also assumed that the pile-up heights would follow Jardret's equation. However, there is high probability that side pile-ups would have an uneven distribution due to

the non-symmetrical geometry of the scribing face for the scribing force model, which might result in discrepancies. It is required to address these assumptions in further studies to develop more accurate scribing force model.

3.5 Chapter Summary

In this chapter, a scribing force model was developed for polymeric CNT nanocomposites, especially MWCNT-PS. Micro scribing experiments identified resulting scribing forces at different CNT concentrations and alignments, while micro indentation experiments identified material hardness and modulus of elasticity at different CNT concentrations. Analyzing the experimental data provided linear polynomial equations for scribing parameters under given conditions, which would provide a method for prediction of scribing forces from indentation experiments.

The proposed scribing model contributed in further understanding of the material removal/deformation procedure during micro-scribing of polymeric CNT composites. In the future, fabrication of micro-sized features on polymeric CNT nanocomposites with aligned CNT orientation can be planned for more efficient machining with the ability to predict not only scribing forces but any mechanical machining techniques based on the fundamental parameters of machining characteristics, by performing non-destructive indentation experiments.

Studying of polymeric CNT nanocomposites have also determined that CNT nanocomposites become hard and brittle with addition of CNTs into polymer matrices. Current study of scribing force model may assist in selection of optimized parameters; however, high scribing forces and geometric inaccuracies due to pile-ups cannot be eliminated. In the next chapter, a new micro mechanical machining method is introduced to overcome such issues.

CHAPTER 4. DEVELOPMENT AND INVESTIGATION OF EVM SYSTEM

Elliptical vibration machining (EVM) is a technique developed to improve machining efficiency. It is especially useful in micro mechanical machining as it can be used to reduce forces during the machining process, increasing the tool life and improving the surface quality. It is also applicable in fabrication of functional engineered surfaces, as it is capable of creating micro patterns with each successive rotation of the tool. However, further investigation is still required to fully understand the mechanism behind experimental results. There had been few models to describe how the EVM process reduces forces, one of them considering the upward motion of EVM assisting chip removal, and the other considering the reduced effective chip thickness at each successive rotation of the tool.

In this chapter, a new design of EVM system is proposed and developed. The system is capable of amplifying its motion without limiting its operational frequency at a natural frequency, very versatile in its range of motion; it can be used at various experimental conditions to compare current models of EVM process, leading to the development of a new model and understanding the mechanism of EVM process. Its versatility would also allow use of the EVM system in fabrication of dimpled surfaces with functionalities. A control algorithm of the developed EVM system is established by first estimating its range of motion analytically, then experimentally verifying and compensating the error due to dynamic effects of vibration frequency. The system is used to study the effects of changing feed rate and vibration frequency in machining forces. The test was also performed to create dimpled surface to verify its

functionality.

4.1 Development of EVM System

In this section, the developed EVM system is described. Its ranges of motion and amplification ratios are verified, and the control algorithm is described in mathematical equations. The algorithm first assumed perfectly rigid frame and freely rotating joints, however, the system has flexure joints to translate piezoelectric linear actuations into elliptical motion. Experiments were performed in varying vibration frequencies to analyze the error and the results were used to compensate the control algorithm.

4.1.1 Design of EVM System

The EVM system's design concept is based on the non-resonant EVM systems, especially Cerniway's [Cerniway 2001], where two piezoelectric actuators apply linear vibrations at a certain phase, translating the actuations into elliptical motions (see Figure 2.7). In the new system, a flexure joints are adopted instead of rotating joints. Using the flexure joints, the system can be made out of a single piece of material without any joining procedures in order to provide the maximum fatigue life. Such design would also allow simple manufacturing procedures involving only water-jet machining and drilling.

Two pieces of piezoelectric actuators (Thorlabs PZS001) are used to provide the required actuations. These piezoelectric actuators have actuation to input voltage ratio of 0.122 μm/V and the maximum displacement of 20 μm. Use of stacked actuators can increase the maximum range of actuation; however, the stacked actuators are prone to thermal degradation as heat accumulates during continuous operations. Instead of using stacked actuators, the concept of leverage was implemented to amplify the range of motion. Figure 4.1 illustrates concept designs in the

iteration process. Each design concept was simulated using commercial finite element analysis (FEA) tool (ANSYS^{TM}). Additional flexure joints were added and various ratios of leverage were tested by changing the location of actuators (indicated by F_a and F_b), length of arms, thickness of arms, radius of cut in flexures and materials. It was found that the effect of the bending is really severe, and it could only be compensated by having really large lever arms.

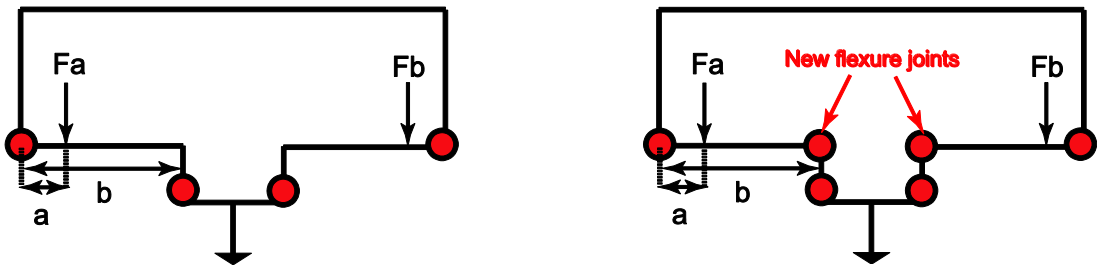

(a) First concept design (b) Second concept design

Figure 4.1 Concept designs for EVM system structure

Through iteration, the final design was proposed as shown in Figure 4.2. The system has width of 145 mm, height of 95 mm and thickness of 9.52 mm (3/8") where material is aluminum 6061 alloy. In this design, actuation is applied upward and translated to downward motion through the first flexural joints (*J1*) attached to the top of the structural frame. Flexural joints *J2* and *J3* assure two actuations at different phase to be applied without straining each other.

The system achieved an amplification ratio of approximately 2.0 from FEA simulation for both horizontal and vertical directions. The horizontal amplification ratio is measured by the ratio of maximum horizontal displacement of the tool tip in *x*-axis versus the amplitude of piezoelectric actuator vibration. It is achieved when only one actuator is actuating while the other is not. The vertical amplification ratio is measured by the ratio of maximum vertical displacement of the tool tip in *z*-axis versus the amplitude of the piezoelectric actuator vibration. It is achieved when both actuators are actuating at the same time, without any phase difference.

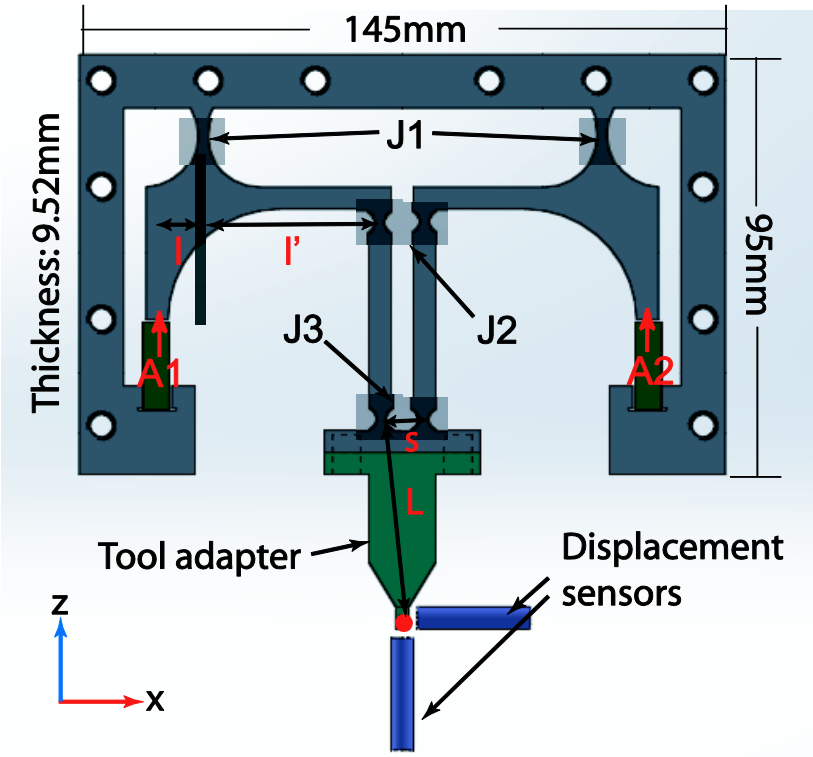

Figure 4.2 Shcematic of final design of EVM system

In order to determine the range of motion of the developed EVM system, experiments were performed to test the effects of input voltages and frequencies. Pick to pick voltages of 20, 60 and 100 V were applied with frequency of 1, 25, 50, 75, 100 and 150 Hz. Input signals for piezoelectric actuators were generated, and the capacitance sensor signals were captured using dSpace (RTI-1305) real-time workshop which is configured with Matlab Simulink™. The amplification ratios, both horizontal and vertical, are shown in following Tables 4.1 and 4.2.

It was shown that both amplification ratios were increased when higher input voltage was applied. The horizontal amplification ratio was observed to be more than 2, reaching as high as 7.35 at higher frequencies.

Table 4.1 Experimental horizontal amplification ratio

Drive voltage (V)	Input displacement (μm)	Amplification ratio at varying frequencies					
		1 Hz	25 Hz	50 Hz	75 Hz	100 Hz	150 Hz
20	2.44	2.3467	2.2904	2.3139	2.5859	2.9986	5.6220
60	7.32	2.7177	2.6255	2.6322	2.8970	3.3749	6.7955
100	12.2	2.9336	2.8507	2.9051	3.1093	3.6951	7.3480

Table 4.2 Experimental vertical amplification ratio

Drive voltage (V)	Input displacement (μm)	Amplification ratio					
		1 Hz	25 Hz	50 Hz	75 Hz	100 Hz	150 Hz
20	2.44	1.0772	0.9896	0.9537	1.0037	1.0037	0.9349
60	7.32	1.2038	1.0970	1.0391	1.0907	1.1079	1.0770
100	12.2	1.3014	1.1979	1.1335	1.1819	1.2130	1.1807

The vertical amplification ratio decreased with increasing frequencies, reaching as high as 1.30 at the low frequency of 1 Hz. Though the vertical amplification is small, the angle of toolpath can be adjusted by changing the phase angle or how the system is attached to the post. Therefore, it is concluded that a versatile system with varying amplification ratio has been developed.

4.1.2 Development of Control Algorithm

Based on the geometries shown in Figure 4.2, a kinematic model was developed to estimate the ranges of motion in EVM at each input parameters. The kinematic model describes the mathematical relationship between resulting toolpaths and given input parameters. Thus the model would enable optimal selection of input parameters for desired toolpath geometries.

The kinematic model can be represented by the following equations with the given sinusoidal amplitudes of piezoelectric actuators and the phase difference between the two actuators. The tilt angle of the elliptical toolpath is depicted based on dimensional constants

illustrated in Figure 4.2:

$$\chi = \frac{1}{2}\tan^{-1}\left(\frac{2G_1G_2(A_2^2 - A_1^2)}{G_1{}^2(A_2^2 + A_1^2 - 2A_1A_2\cos\varphi) - G_2{}^2(A_2^2 + A_1^2 + 2A_1A_2\cos\varphi)}\right) \tag{4.1}$$

$$\begin{aligned} G_1 &= \frac{l'L}{ls}\sin(\arccos(\frac{s}{2L})) \\ G_2 &= \frac{l'L}{2lL} \end{aligned} \tag{4.2}$$

where α and β are representing geometric constants described in Figure 4.2. Once the tilt angle χ is identified through Eq. 1, the major (a) and minor (b) radii of the elliptical toolpath can be identified given as:

$$\begin{aligned} a &= \sqrt{1/(\kappa_1\frac{(1+\kappa_2)}{2} + \kappa_3\frac{(1-\kappa_2)}{2} - \kappa_4\kappa_2)} \\ b &= \sqrt{1/(\kappa_1\frac{(1-\kappa_2)}{2} + \kappa_3\frac{(1+\kappa_2)}{2} + \kappa_4\kappa_2)} \end{aligned} \tag{4.3}$$

The parameters, κ_1, κ_2, κ_3 and κ_4 are the abbreviated functions dependent on input parameters, represented by the following equations:

$$\begin{aligned} \kappa_1 &= \frac{A_2^2 + A_1^2 + 2A_1A_2\cos\varphi}{4G_1{}^2A_2^2A_1^2\sin^2\varphi} \\ \kappa_2 &= \sqrt{\frac{1}{1+\tan^2 2\chi}} \\ \kappa_3 &= \frac{A_2^2 + A_1^2 - 2A_1A_2\cos\varphi}{4G_2{}^2A_2^2A_1^2\sin^2\varphi} \\ \kappa_4 &= \frac{(A_2^2 - A_1^2)\tan 2\chi}{4G_1G_2A_2^2A_1^2\sin^2\varphi} \end{aligned} \tag{4.4}$$

Using the equations, the theoretical toolpath at any given input parameters can be plotted. The change in toolpath geometries at different ratios of actuation amplitudes is illustrated in Figure 4.3, where the phase angle was maintained constant. On the other hand, Figure 4.4 illustrates resulting geometries at varying phase angles with constant ratios of actuation

amplitudes.

Both the drive amplitudes and phase angle affect the tilt angle and the size of toolpath at the same time, thus the combination of input parameters is important to have a desired toolpaths. According to the kinematic model, the major radii *a* increases and the minor radii *b* decreases as the phase angle increases from 0 to π. The increase in the ratio of amplitudes would result in increased radii, but the relationship can be reversed if the phase angle is low enough. It was notable that the X-axis range of motion was larger in comparison to the Z-axis.

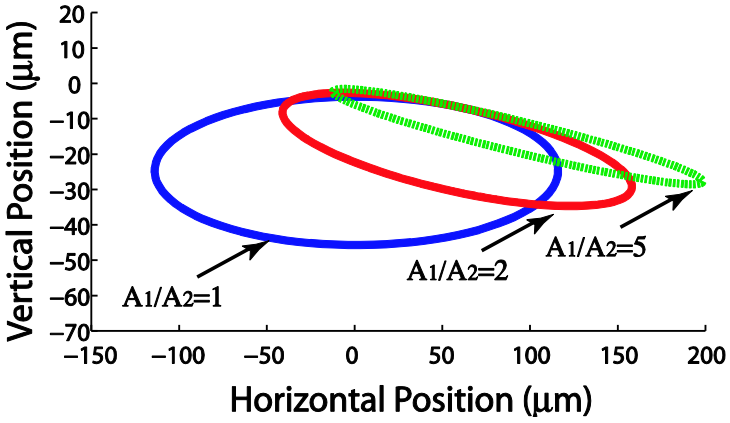

Figure 4.3 Theoretical toolpath geometries with varying ratio of amplitudes ($\varphi=\pi/3$)

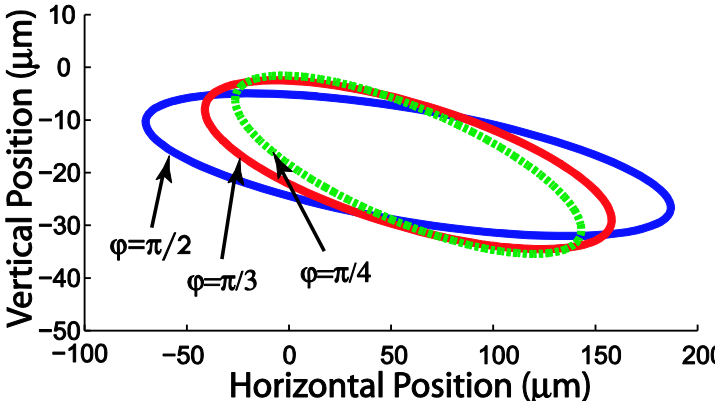

Figure 4.4 Theoretical toolpath geometries with varying phase angles ($A_1/A_2=2$)

There are several assumptions associated with the proposed kinematic model. The model assumes the rigidity of beams and elements, but in reality, such assumptions lead to errors between the resulting and expected toolpaths since the system is using flexure hinges instead of rotating joints. The toolpath would not follow the model exactly, though it would follow the general tendency. It is important to study the discrepancy and how it is related to input parameters, thus the kinematic model can be updated with calibration factors.

In this study, experiments were performed to find the amplification ratio at varying frequencies and input voltages, while the phase angle and amplitude of input voltages were limited to constant values to maintain perfect circle. Peak to peak voltages of 20, 60 and 100 V were applied to the both actuators, maintaining circular toolpath geometry, as well as the varying vibration frequencies of 1, 10, 25, 50, 75, 100, 125 and 150 Hz. Resulting amplification ratios are illustrated in Figure 4.5.

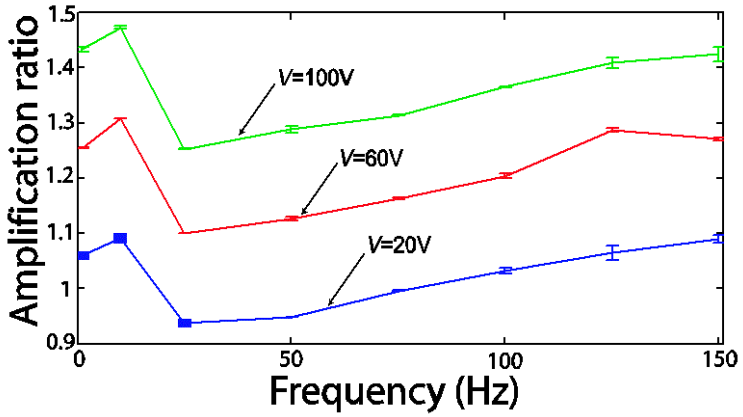

Figure 4.5 Experimental amplification ratio with perfectly circular toolpath ($\varphi=3\pi/16$, $A_1=A_2$)

The highest amplification ratio was achieved at the low frequency, and then the amplification ratio rapidly decreased near 25 Hz but slowly increased after. It is important to note that the amplification ratio, on top of the absolute toolpath size, was increased as the input

voltage was increased while maintaining similar tendency over the frequency.

In order to correct the toolpath generated from the kinematic model with the experimental results, we have applied the empirical constant λ which is multiplied to a and b in equation (4.3). The empirical constant λ was identified using the curve fitting method, as a function of the vibration frequency f and the input voltage V ($V=A_1=A_2$). Perfectly circular toolpath geometry is important as it can be studied in terms of milling, where the cutting edge shows similar toolpath geometry.

$$\lambda = (0.9 + 0.00975V) \times 0.003e^{0.0444f} + (0.85 + 0.005V) \times 1.875e^{0.001407f} \quad (4.5)$$

The limitation in the empirical factor is that it only applies if the amplitudes of input voltages for both piezoelectric actuators are equal to each other. Further analysis is required to obtain the relationship between the vibration frequencies and resulting geometries when the amplitudes of input voltages for two actuators are different from each other.

4.2 Micro Cutting Tests Using EVM

The system was verified of its functions through actual cutting experiments. Orthogonal micro machining tests were performed with and without elliptical vibrations, comparing the resultant cutting forces. A surface pattern was generated and verified of its surface geometry as well.

4.2.1 EVM Experimental Setup

The experimental apparatus include the EVM system, the diamond tool and the workpiece. The 3-axis micro-milling CNC machine developed in-house was utilized to apply the

required feeding motion. A 3-axis piezoelectric force sensor (Kistler 9256C2) was mounted on top of the stage, allowing force measurements in 3-axis during the experiments. The forces were measured and recorded at 1 kHz sampling frequency. While the EVM system creates elliptical vibration, the stage of micro-milling CNC machine provides a single axis feeding motion at predefined feed rates.

An orthogonal diamond tool is held tight using an adapter built in-house, which is mounted on the EVM system. The tool used in this experiment is a single crystal diamond orthogonal tool (ALMT UAF00023) with edge radius of 0.10 μm, 1.15 mm width and inherent positive rake angle of 15 degrees. The orientation of the tool is illustrated in Figure 4.6, where the tool is tilted 15 degrees to achieve actual rake angle of 0 degrees.

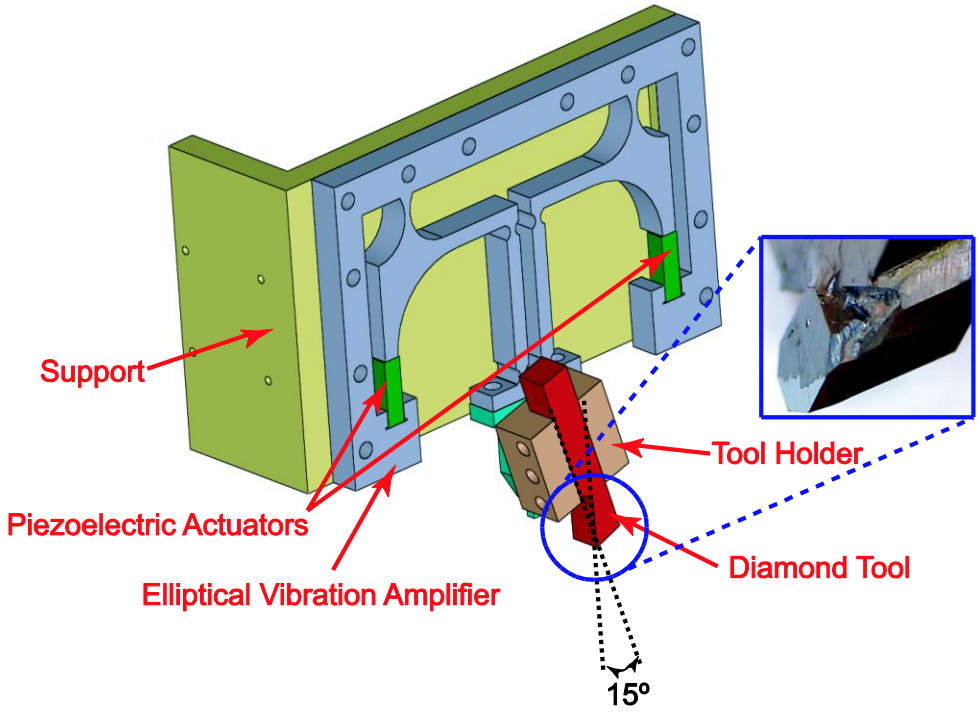

Figure 4.6 Schematic of experimental apparatus

The machinable wax workpiece was prepared to test the EVM system. The surface was

pre-machined prior to the experiment. The elliptical vibration machining experiments were performed first by bringing the tool to the contact with the workpiece surface to set the vertical datum. The contact is identified by observing the force sensor signal. Once the contact is confirmed, the workpiece sample is moved in x-axis to scratch the surface and cut out any materials above the z-axis datum.

4.2.2 EVM Machining Experiments

The EVM processes are known to reduce machining forces in comparison to the orthogonal cutting. In this study, EVM micro cutting experiments were performed to see the effects of EVM in comparison to the conventional orthogonal cutting where vibration is not applied.

A circular toolpath with radius of 5 µm was maintained at all conditions. Three different vibration frequencies (1, 10, 50 Hz) were tested on top of the conventional orthogonal cutting without any vibration, where the horizontal feed rate was maintained at 50 µm/s. The depth of cut was maintained at 10 µm in all conditions.

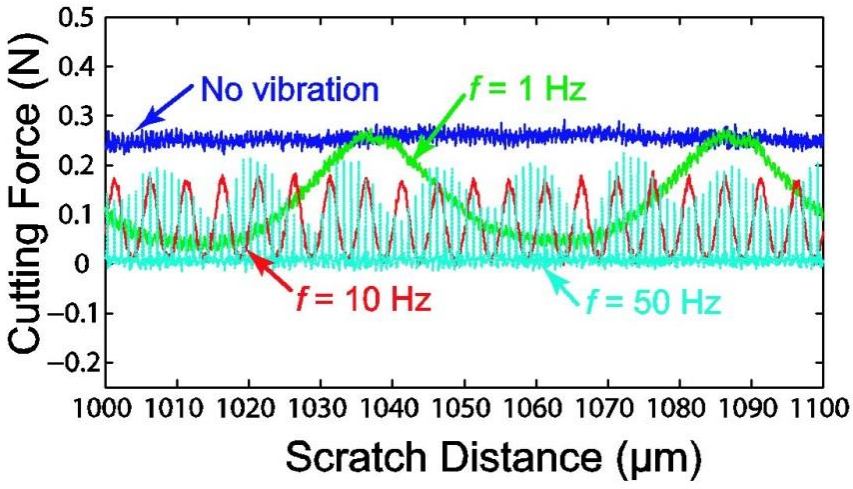

Figure 4.7 Horizontal cutting forces at varying frequencies

The resulting forces are shown in Figures 4.7 and 4.8. Figure 4.7 illustrates horizontal cutting forces obtained from EVM process at varying frequencies. It was observed that horizontal cutting forces decreased with vibration in comparison to orthogonal cutting without any vibration. Increase in vibration frequencies further reduced average cutting forces.

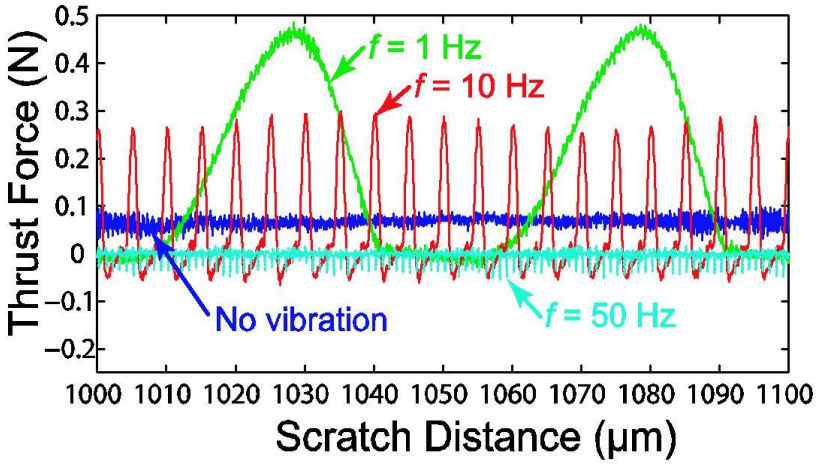

Figure 4.8 Vertical thrust forces at varying frequencies

Resulting vertical thrust forces are illustrated in Figure 4.8. Unlike the cutting forces, low frequency vibrations at 1 and 10 Hz resulted in higher average forces than the cutting without vibration. However, the forces decreased as the frequency was increased, resulting in average forces lower than the cutting without vibration at 50 Hz of vibration frequency. It is notable that the lowest peaks of the thrust forces become negative values. This was reported in Shamoto and Moriwaki [1992] as well, where the tool applies upward forces assisting chip removal. This phenomenon verifies that the EVM system is functioning to reduce forces with high frequency vibration.

Investigating dynamic forces at varying frequencies is the first step to understand the mechanics behind EVM process. The study has to be further extended to understand how the forces affected by increased frequencies, in relation to the effective chip thickness, effective tool

rake angle and velocity.

The ability of the EVM system to generate surface pattern was also tested. As it is described in Figure 4.9, the EVM process can be used to generate surface pattern where each successive rotation cuts into material without crossing each other.

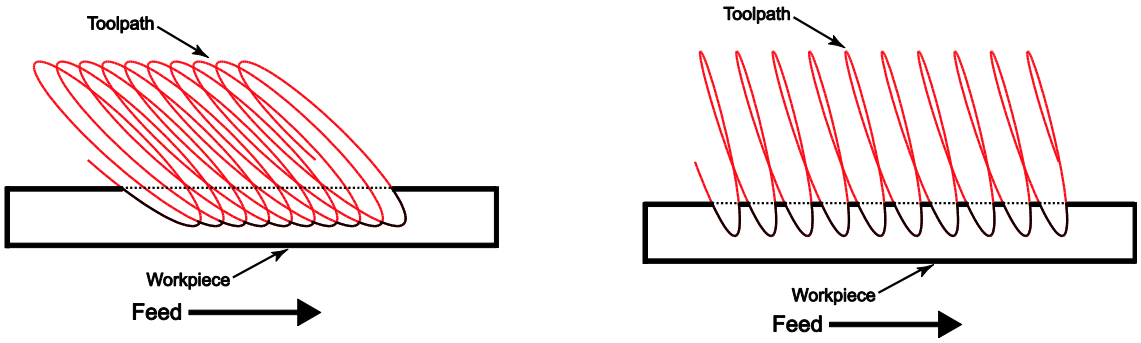

(a) Toolpath at relatively low feed rate (b) Toolpath at relatively high feed rate

Figure 4.9 Comparison of toolpath at different feed rates

The surface pattern generation ability was tested at the feed rate of 300 µm/s. The vibration frequency was maintained constant at 10 Hz, depth of cut at 10 µm and the radius of vibration at 5 µm. Under this condition, surface pattern of sinusoidal waves with 30 µm period and 10 µm depth was machined. The surface quality of machined surfaces has been measured using a non-contact measurement method based on the chromatic confocal sensor (STIL CCS OPTIMA CHR150-L). Figure 4.10 shows the plots of the estimated and the measured surface pattern.

The horizontal peak to peak distance was measured to be approximately 30.0 µm, and the peak to valley depth was approximately 10.2 µm. The resulting surface profile matches the simulated surface profile closely with error of 0.2 µm. It was concluded that the EVM system was able to fabricate surface patterns at a fast pace.

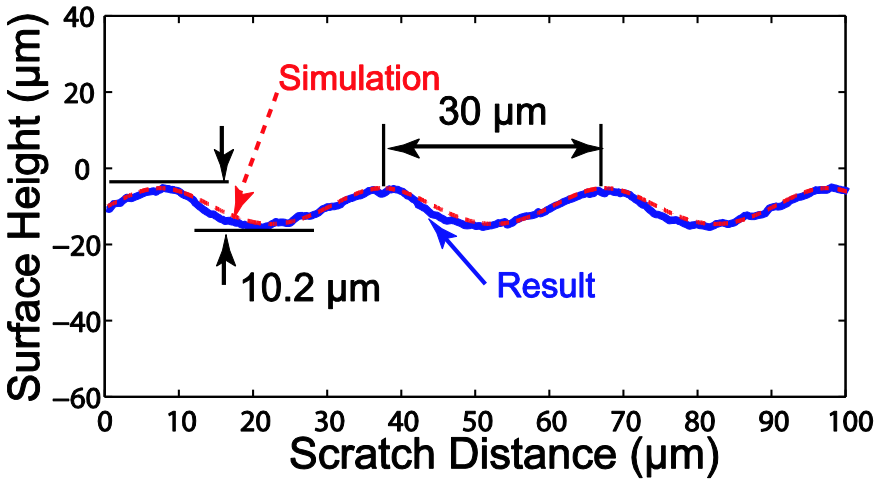

Figure 4.10 Profile of surface pattern along the feed direction

4.3 Chapter Summary

In this chapter, a novel elliptical vibration machining system was developed and experimentally verified. The system has a wide range of operation in both toolpath frequency and geometry, where the control algorithm for circular motion was established in this study. Using this system, elliptical machining experiments were performed at different feed rates and vibration frequencies, and it was identified how machining forces are affected by them. Systems provided in this study can be used in further studies to compare existing force models which were limited in its input parameters due to the experimental apparatus used in each model. Being able to compare models, it is possible to determine which model would fit general conditions more and develop new model incorporating scribing force model developed in the chapter 3.

In this chapter, the capability of the developed EVM system to generate surface pattern using high feed rate was demonstrated as well. Only a small percentage of geometrical error was measured; it opens up possibilities in fabrication of functional surfaces with micro-scale features utilizing the EVM technique.

CHAPTER 5. CONCLUSIONS

Summary and the novel contributions of this study are presented in this chapter, explaining the significance of the study. It has contributed to the scientific community in micro mechanical machining field by providing a novel mechanistic force model, relating the material properties obtained from micro indentation to the scribing forces with respect to the alignment of the CNTs in polymeric CNT nanocomposites. The study also provided a novel and versatile EVM system, where the system is proved to have wide range of operations in terms of toolpath geometries and vibration frequencies. Assumptions and limitations involved with the modeling and experiments are also discussed. The chapter concludes with possible future work that can improve this study further.

5.1 Summary

Demand for micro mechanical machining has risen in past decades due to its advantages over other micro manufacturing techniques, as it is capable of fabricating complex 3-D shapes with high efficiency in time and cost, almost unlimited choice of material. However, applications of micro mechanical machining is not as simple as applying conventional mechanical machining, as there are differences in micro and macro scale machining processes. The tool edge cannot be considered ideally sharp as it was in conventional macro scale model, and there are material plowing, elastic recovery, pile ups and grain boundaries all affecting modeling of micro scale mechanical machining.

One of the different aspects of research in micro mechanical machining is studying the

machining characteristics of materials with unique properties, such as the polymeric CNT nanocomposites – a composite material that can have anisotropic material properties depending on the CNT alignment. Another aspect of micro mechanical machining is studying mechanism of non-conventional micro mechanical machining technique, such as the elliptical vibration machining (EVM) technique. The EVM process applies bi-axial vibrations to conventional machining technique, reducing average forces applied during the process. Both aspects of research in micro mechanical machining require development of custom experimental apparatus to investigate interaction between tools and materials. Understanding these two aspects of micro mechanical machining would result in optimization of machining parameters with higher efficiency, thereby expanding usage of micro mechanical machining applications currently limited by gap of knowledge between the conventional machining and micro machining.

Polymeric CNT nanocomposites have special material properties as CNTs provide electrical and thermal conductivities while improving its mechanical properties as well. Such characteristics can be specialized even further with alignment of CNTs in certain direction, which can be partial obtained through micro injection molding process. Electrical conductivity, thermal conductivity, and bulk material strength exhibit anisotropy with the partial alignment [Arjmand et al. 2011, Mahmoodi et al. 2012]. Micro mechanical machining is a method to post-process the injection molded polymeric CNT nanocomposites as mechanical machining can fabricate complicated features without disturbing CNT alignments. While there had been few researches on machinability of polymeric CNT nanocomposites in micro milling process [Mahmoodi et al. 2012], there was no study correlating material properties and scribing forces in a mechanistic force model with respect to the CNT concentrations and direction of alignments.

In this study, a novel micro indenter-scriber system was developed. Micro scribing

experiments were performed on MWCNT-PS samples in varying CNT concentrations and feed directions, parallel and perpendicular to the CNT alignment. Micro indentation was also performed on these samples to find the material hardness and modulus of elasticity, mainly utilizing analytical steps proposed by Oliver and Pharr [Oliver and Pharr 2004]. Based on the experimental results from micro scribing and indentation experiments, a mechanistic force model was proposed.

The elliptical vibration machining technique was also investigated to meet the demand of more advanced machining technique, reducing machining forces and unwanted pile-ups from scribing. The EVM process was proposed in extension of its predecessor technique, linear vibration assisted machining, where bi-axial vibration was applied. Many researchers reported that this technique can be used to reduce average machining forces in comparison to the conventional scratching techniques, thus resulting in reduction of tool wear and improved surface finish. Such trait makes this technique especially suitable for micro mechanical machining application where the fabrication methods are susceptible to excessive cutting forces and tool breakages. Some researchers have investigated dimple machining using EVM technique to create functional surfaces as well, but excessive amount of forces are applied. Understanding the force model in EVM process is important to set machining parameters efficiently.

There are currently two different ideas explaining how EVM technique reduces forces. One of them is that the elliptical toolpath applies upward friction in assistance to chip removal, thereby reducing overall cutting forces. On the other hand, there is an explanation that force is reduced as the dynamic uncut chip thickness is reduced as the tool is cutting away smaller volume of the material at each cycle, similar to the milling process. In order to understand EVM mechanics further, a versatile EVM system is required, thus it could mimic and perform

comparative analysis of experimental conditions stated in different theories. Furthermore, the new system could perform experiments in wide range of experimental conditions to establish a more general force model to explain EVM mechanics.

In this study, a novel EVM system was designed and fabricated by taking advantages of resonant and non-resonant EVM systems. Its ranges of motion were mathematically analyzed assuming rigid bodies and freely rotating joints; then the equation was compensated by acquiring experimental ranges of motion at varying vibration frequencies to establish the control algorithm.

The developed EVM system was verified of its function by cutting experiments at different vibration frequencies. It was also tested if the system is capable of creating micro surface patterns at a relatively high feed rate.

5.2 Novel Contributions

This study provides insight into micro scribing of injection molded polymeric CNT nanocomposite by developing a mechanistic force model, correlating forces and material properties. It also proposed a versatile EVM system and verified its functionalities in machining with reduced forces and creating dimples at high feed rate. The novel contributions of this thesis can be listed as following.

5.2.1 Development of Novel Mechanistic Force Model of MWCNT-PS

A custom micro indenter-scriber system was developed to be used in investigation of MWCNT-PS through micro scribing and indentations. Being able to measure forces in 3 axis and applying displacements in 3 axis, the system allows micro scribing and indentation experiments to be performed in one experimental set-up. This improves the efficiency in time it takes to

perform experiments, but more importantly, using a same tool in both indentation and scribing allows the two data to be correlated.

First, micro scribing and indentation experimental results were analyzed to understand the scribing characteristic and identify the material properties. From the scribing experiments, it was found out that a small loading of CNT (i.e. 0.5 wt.% CNT) resulted in higher cutting (50% increase) and thrust forces (95% increase) compared to the pure PS. In addition, the apparent friction coefficient showed the lowest value. The differences between cross-flow and in-flow scribing in cutting and thrust forces were small at low CNT concentration (0.5 wt.%), but the difference was more significant at higher CNT concentration (0.5 wt.%). A higher cutting and thrust forces were observed for scribing in the cross-flow direction compared to the in-flow direction especially for 5 wt.% CNT composites. This is due to higher interaction between the CNTs and the tool which may cause breakage of CNTs.

Micro-indentation experiments were also performed on the CNT composite samples to identify the modulus of elasticity and hardness at varying CNT concentrations. Hardness was highest with small addition of CNT (0.5 wt. %), reaching up to approximately 270 MPa. However, higher the CNT concentration, the hardness decreased; as MWCNT-PS with 2 wt.% CNT load exhibited 200 MPa and MWCNT-PS with 5 wt.% CNT load exhibited 150 MPa of hardness. The above hardness was all measured with the maximum indentation at 5 μm, similar to the depth of cut in scribing experiments. The modulus of elasticity were ranged from 3.2 to 4.0 GPa, and there was no specific order found in them.

It is suspected that the dispersion of CNTs has a strong relationship to the results. At higher CNT concentrations, CNTs tend to agglomerate due to Van der Waal's force and the agglomerates would act as stress concentrators which would result in crack initiation and

propagation. In addition, the difference of scribing forces in cross-flow and in-flow orientations was more significant at higher CNT concentrations while the orientation of CNT produced negligible differences in the ratio of the cutting and thrust forces (i.e. the apparent friction coefficient).

Comparative analysis of MWCNT-PS at different CNT concentrations using micro scribing and indentation techniques provided unique information of the given material; the significance of this study lies within a novel mechanistic force model correlating these information. By establishing linear equations of relationship between the indentation material properties and scribing forces, it has been made possible to predict scribing forces from varying concentrations with only the indentation experiments.

The novel mechanistic force model consists of three different unknown parameters: shearing coefficient, plowing coefficient and adhesion friction coefficient. In order to solve for these three unknowns, three axis of force measurements were required; therefore, the scribing was performed with the tool oriented so that the normal vector of the tool face and the scribing direction would have deviation of 30 degrees of angle. This scribing direction allowed for the measurement of the three axes of forces due to its asymmetric geometry. Two scribing feed directions were applied: parallel to the CNT alignment (in-flow) and perpendicular to the CNT alignment (cross-flow). The results were compared between the scribing directions, as well as between different CNT concentrations.

The experimental results were analyzed for the scribing force model; and, it was determined that the shearing coefficient, κ_s, increased with the addition of CNTs in the cross-flow direction, but decreased during in-flow scribing. This phenomenon confirms that scribing or machining parallel to the CNT flow would result in low shear strength, even though the CNT

concentrations are the same. The plowing coefficient, κ_p, increased with the increasing additions of CNT in both scribing orientations; however, cross-flow scribing exhibited higher plowing coefficients at high CNT concentrations, such as 5.0 wt.%, compared to in-flow scribing. The adhesion friction coefficient, μ_a, decreased with increasing CNT concentration, with cross-flow scribing showing significantly higher friction coefficients at lower CNT concentrations. At high CNT concentrations (i.e. at 5.0 wt.%), the difference in the adhesion friction coefficients between the two scribing orientations was negligible.

Three coefficients could be expressed in linear equations in relationship to the exponential to the ratio of the modulus of elasticity and hardness. Using this linear relationship, the shearing, plowing and adhesion friction coefficients can be obtained as long as the material hardness and modulus of elasticity is known, thereby predicting forces.

In order to verify the model, the scribing force model was used to estimate forces where MWCNT-PS sample with 2 wt.% CNT load, scribing in-flow and cross-flow. The estimated forces were compared to the experimentally obtained forces to find the errors. In the cross-flow scribing experiments, the estimated forces from the model had errors of 1.60, 9.66 and 35.3 % for F_X, F_Y and F_Z, respectively. In the in-flow scribing experiments, the estimated forces from the model had errors of 6.22, 7.32 and 37.9 % for F_X, F_Y and F_Z, respectively. While the estimation in horizontal forces had small errors, estimation in vertical forces showed significant errors, which would need further investigation.

The proposed scribing model, however, allow fairly accurate prediction of scribing forces especially in horizontal directions, from material properties obtained from micro indentations. Understanding the effects of CNT concentration and orientation in scribing both qualitatively and quantitatively, more efficient micro scribing is capable. Furthermore, the fundamental

knowledge of the tool-material interaction found from scribing can be adopted into more complicated micro mechanical machining operations – such as micro milling or EVM process.

5.2.2 Development and Verification of Versatile EVM System

A versatile EVM system was developed using a monolithic aluminum frame and two piezoelectric actuators. The EVM system is able to mechanically amplify the motion of actuators through the concept of leverage and dynamic properties of flexural hinges, generating elliptical motions in wide range of amplitudes and frequencies. From the experiment, it was found out that the horizontal amplification ratio ranged from as small as 2.35 to as high as 7.35. The vertical amplification ratio was relatively small, ranging from 0.93 to 1.30, but the angle of the toolpath can be varied.

A kinematic model of toolpath was developed assuming rigid bodies and freely rotating joints, where the geometries of toolpath were varied at changing ratio of actuation amplitudes and the phase angle of vibrations in two actuators. Dynamic effects of vibration at flexure joints were taken into account. An equation of non-linear empirical constant λ was identified in relation to the vibration frequencies and input voltages.

Experiments were performed to verify the functionality of the developed EVM system. At varying frequencies (0, 1, 10 and 50 Hz), a machinable wax was machined using the system while measuring cutting and thrust forces. It was found that cutting forces were decreased at higher frequencies, as the mean cutting force was 0.25 N at no vibration, 0.16 N at 1 Hz, 0.10 N at 10 Hz and 0.02 N at 50 Hz of vibration frequencies. Thrust forces also decreased with increasing vibration frequencies, but the mean forces were smaller than cutting without vibration only at 50 Hz. Mean thrust forces was 0.07 N at no vibration, 0.25 N at 1 Hz, 0.10 N at 10 Hz and 0.01 N at 50 Hz. This might be the result of the forces applied to the flank of the tool, but

requires more investigation. Notably, all thrust forces showed that they experience negative thrust force – which is force applied upward, assisting the chip removal.

The ability to fabricate surface pattern was also tested. A sinusoidal pattern with 30 µm period and a 10 µm depth was fabricated by applying feed rate of 3000 µm/s with 10 Hz of vibration frequency. From the surface measurement, the vertical error was less than 0.2 µm.

Thus, it can be concluded that a novel EVM system was developed with wide range of motions, operating outside of natural frequency of the system. The system is applicable to study the mechanism of the EVM process, especially in comparing two models previously proposed by Shamoto and Moriwaki [Shamoto and Moriwaki 1994] and Cerniway [Cerinway 2001], leading to the development of new model and thereby acquiring deeper understanding of the EVM process.

5.3 Assumptions and Limitations

There are several assumptions and limitations associated with the study and they need to be addressed to improve the study in future. They range from simple measurement errors that were not considered to assumptions in modeling due to the lack of relevant knowledge at the current stage.

MWCNT-PS sample used in the study has nonlinearity in material itself as the CNTs could not be dispersed perfectly. Micro scribing experiments were performed in limited experimental conditions, where machining parameters other than the material properties can affect scribing forces. The EVM control algorithm was experimentally verified only in limited setups, and the design has issues due to the tool deflection. They have to be reviewed to identify the possible sources of error and what can be done further to improve this study.

During the development of the mechanistic model for micro scribing of MWCNT-PS, there as one critical assumption: constant flow stress was applied at any moment of scribing on the material surface. Since MWCNT-PS is a composite of CNT fillers and polystyrene matrix, material properties may differ by each location depending on its relative position to CNT fillers. Some degrees of agglomeration of CNT fillers were identified through TEM images of workpiece samples, however, the effects of agglomeration were not considered either. CNT delamination or pull-outs may cause changes in forces.

In the mechanistic model for micro scribing, the geometries of diamond tools were assumed to be constant. Such assumption may be subject to errors, as the diamond tool may not be aligned perfectly with respect to the CNT flow directions and there are possible tool wears through repetitive experiments. This would affect force measurements in both indentation and scribing experiments, which might cause errors in tool geometries.

The mechanistic modeling of micro scribing used in this study was limited in the scribing feed rate. All scribing experiments were performed in 1μm/s scribing feed rate, which is relatively slow feed rate in comparison to the depth of cut (5 μm). It is well known that feed rate affects cutting forces in non-linear behaviour. Further study is required to expand current scribing force model to cover all scribing feed rates.

The EVM system developed in this study has many challenges associated with the design. The design process was limited by the computational power; accurate estimation of dynamic behaviour under vibration was not achieved through FEA. It requires large amount of repeated experiments at varying conditions to create control algorithm of the system. An empirical factor was introduced to consider varying amplification ratios at different vibration frequencies and input actuation voltage, but under limited condition. It is applicable only if circular toolpath is

generated (input actuations of both piezoelectric actuators are same, and the phase angle is constant at 3/16 π).

The already limited control algorithm is further limited due to the design itself. While the control algorithm is fairly accurate during the test without cutting any material, highly flexible design is susceptible to tool deflection. Experiments performed in this study included testing the system's capability in surface pattern generation, where the error was within 2% of the desired toolpath.

The flexibility of the system may cause errors in force modeling, and the comparative force analysis performed in this study may have some errors as well. During the orthogonal cutting process, the tool experiences larger forces, and there is no consideration in tool deflection. The tool rake angle is considered perfectly orthogonal to the workpiece feed direction during orthogonal cutting. In reality, the tool experiences deflection depending on the amount of force applied and the magnitude of bending could have been different in orthogonal cutting and EVM processes using this system. Experimental modal analysis using impact hammer has found that the system has static horizontal stiffness of approximately 55 μm/N. During the non-vibrational orthogonal cutting process, the cutting force has reached as high as 0.5 N and it could have altered rake angle due to tool deflection, thereby affecting the measured forces. The displacement of tool was not measured during the cutting process, and it would be beneficial to monitor and study the vibrations and in-situ tool tip motion during the cutting.

Force measurements during EVM processes has proved that there were vibrations at high frequency on top of the input vibration frequencies, and these might be due to the flexible system. For more accurate studies of EVM processes, control algorithm is required to be further modified to include the tool deflections in toolpath estimation.

Assumptions and limitations of this study were discussed in detail. While this study provides some novel contributions in understanding of micro mechanical machining, it identified more to be studied further. Addressing assumptions and limitations listed in this section set a guideline for future works. Assumptions will be verified whether the assumption was valid or not, and limitations in the model would be alleviated, leading to a more general modeling than specific conditions.

5.4 Future Work

This study provided some insight into mechanistic modeling of micro scribing polymeric CNT nanocomposites and the EVM processes. In this section, possible future works are introduced, studies that are required to improve the current understanding and to extend it.

First priority in the future works is to address the assumptions and limitations discussed previously. In order to improve the mechanistic model of micro scribing of polymeric CNT nanocomposite, anisotropic characteristic of MWCNT-PS (and other polymeric CNT nanocomposites) have to be studied further. Micro injection molding process can be improved further to control CNT dispersion better, however, this is another subject to be studied. This study can be extended further with phase imaging techniques, scanning the surface and identifying gradient of material properties. In order to have phase imaging capability, it is required to have a vibrator to be added to the current indenter-scriber setup, applying vibrations while scanning, measuring the change in vibration modes in the scanned area.

Implementing high-frequency AE signal could be another method to identify interactions between the tool and the material. The current set up limits the AE signal data acquisition to 20 kHz, but it can be improved to have high frequency bandwidth. With frequency bandwidth

higher than 1 MHz, CNT delamination and pull-outs, or crack initiation can be identified. The AE signal analysis can be used in conjunction with force measurements to identify whether there are specific interactions with CNTs other than the material deformation described in current model.

Micro mechanical scribing experiments needs to be studied with more variations of experimental conditions. Different depth of cuts and feed rates can be tested, and the resulting forces can be analyzed to verify whether the current mechanistic model is applicable in general. If not, further investigation is required to implement effects of feed rates and depth of cut to the model, making it more general. The model can be extended even further, performing experiments in other polymeric CNT nanocomposites, such as the polycarbonate based CNT nanocomposites.

The understanding in micro mechanical machining is transferrable to nano-mechanical scribing. The atomic force microscopy is used to perform mechanical scribing as well as scanning the surface. At the nano-metric realm, interaction between individual CNTs and polymer matrices can be identified more clearly, and map of material properties over the entire surface can be obtained from various AFM techniques. Micro scribing model already considers size effects in many aspects. On top of the micro scribing model, forces from molecular interactions have to be considered.

The EVM system developed in this study provides background for the more in-depth studies of micro EVM mechanisms. However, before any of the in-depth study is performed, the limitations in the current EVM system has to be clearly understood. The flexibility of the system requires development of improved toolpath algorithm considering tool deflections, to accurately model the actual toolpath while force is being applied. With the accurate toolpath algorithm, comparative analysis of EVM force models can be performed.

Two types of force models, mainly Cerniway's [Cerniway 2001] and Shamoto and Moriwaki's [Shamoto and Moriwaki, 1994] will be compared to each other in different EVM conditions. The experiments will be performed in varying ratios of vibration amplitude versus depth of cut and horizontal speed ratios to find which model fits better in certain conditions and discuss why. Furthermore, a new force model for EVM process will be developed based on micro milling force model, where the uncut chip thickness and effective rake angles are considered with respect to the dynamically changing tool velocity vector. The new force model will be integrated with the micro scribing force model developed in this study to accurately predict the forces.

Main advantages of EVM process is to reduce applied forces and generate controlled surface after cutting. More specifically, the EVM process can promote chip removal over material deformation even if the material is hard to cut material. The EVM process can be applied to machine grooves and patterns in the polymeric CNT nanocomposites to reduce machining forces and improve the surface finish with chip removal rather than material deformation, which have left side pileups.

The versatile EVM system can be used for other applications as well. I has ability to apply two different actuations with different vibration frequencies, creating complicated geometries other than circle or ellipse. Depending on the ratio of two frequencies, it is possible to create toolpath to cut multiple channels at once or alternating dimples. The toolpath generation algorithm can be expanded further from current model to include toolpaths from asymmetric vibration frequencies. This could be developed into a study of novel technique for functional surface generation with high efficiency.

The surface pattern that was generated using the EVM system, whether it is using the

new asymmetric vibration technique or high feed rate as it was introduced in chapter 4, can be a subject to studies as well. One of the most common use of patterned surface is to reduce friction, where dimples act as reservoir for lubricants and trapping wear debris. The surface pattern can be adjusted to control the optical properties such as the reflectivity and refractivity, or change the surface energy – creating super hydrophobic surface. Using the EVM system, different geometries of surface can be generated in short time to study how their functionalities are affected.

In summary, proposed future works suggest to improve the mechanistic force model developed in this study for wider range of applications with higher accuracy. The EVM system control algorithm will be updated, which will be used to develop new force models adopting the knowledge obtained from the mechanistic scribing force model. Thus the EVM process can be applied to cut polymeric CNT nanocomposites for better efficiency. Its versatility allows its application in generation of functional surface patterns, where the study is directly involved with efficient manufacturing of micro components.

REFERENCES

Abassi, S., Carreau, P.J., Derdouri, A. 2010, "Flow induced orientation of multiwalled carbon nanotubes in polycarbonate nanocomposites: Rheology, conductivity and mechanical properties", Polymer, Vol. 51, pp. 922-935.

Ahn, J.H., Lim, H.S., Son, S.M. 1999, "Improvement of Micro-machining Accuracy by 2-Dimensional Vibration Cutting", American Society of Precision Engineers Conference Proceedings, Vol. 20, pp. 150-153.

Arjmand, M., Mahmoodi, M., Gelves, G.A., Park, S.S., Sundararaj, U. 2011, "Electrical and electromagnetic interference shielding properties of flow-induced oriented carbon nanotubes in polycarbonate", Carbon, Vol. 49, pp. 3430-3440.

Biercuk, M.J., Llaguno, M.C., Radosavljevic, M., Hyun, J.K., Johnson, A.T., Fischer, J.E. 2002, "Carbon nanotube composites for thermal management", Applied Physics Letters, Vol. 80, pp. 2767-2778.

Brinksmeier, E., Glabe, R. 1999, "Elliptical Vibration Cutting of Steel with Diamond Tools", American Society of Precision Engineers Conference Proceedings, Vol. 20, pp. 163-166.

Bucaille, J.L., Felder, E., Hochstetter, G. 2001, "Mechanical analysis of the scratch test on elastic and perfectly plastic materials with the three-dimensional finite element modeling", Wear, Vol. 249, pp. 422-432.

Cerniway, M.A. 2001, "Elliptical diamond milling: kinematics, force, and tool wear", MS thesis, North Carolina State University.

Chae, J., Park, S. S., Freiheit, T. 2006, "Investigation of micro-cutting operations", International Journal of Machine Tools & Manufacture, Vol. 46, pp. 313-332.

Chang, T.-E., Kisliuk, A., Rhodes, S.M., Brittain, W.J., Sokolov, A.P. 2006, "Conductivity and mechanical properties of well-dispersed single-wall carbon nanotube/polystyrene composite", Polymer, Vol. 47, pp. 7740-7746.

Chen, W.X., Tu, J.P., Wang, L.Y., Gan, H.Y., Xu, Z.D, Zhang, X.B. 2003, "Tribological application of carbon nanotubes in a metal-based composite coating and composites", Carbon, Vol. 41, pp. 215-222.

Chung, S., Makhar, S., Ackler, H., Park, S. 2006, "Material Characterization of Carbon-Nanotube-Reinforced Polymer Composite", Electronics Materials Letters, Vol. 2, pp. 175-181.

Collins, P.G., Avouris, P. 2000, "Nanotubes for Electronics", Scientific American, Vol. 283, pp. 62-69.

Demczyk, B.G., Wang, Y.M., Cumings, J., Hetman, M., Han, W., Zettl, A,. Ritchie, R.O. 2002, "Direct mechanical measurement of the tensile strength and elastic modulus of multiwalled carbon nanotubes", Materials Science and Engineering A, Vol. 334, pp. 173–178.

Fischer-Cripps, A.C. 2002, "Nanoindentation", Springer-Verlag New York, Inc., New York.

Hokkirgawa, K., Kato, K. 2003, "An experimental and theoretical investigation of plowing, cutting and wedge formation during abrasive wear", Tribology International, Vol. 21, pp. 51-57.

Jardret, V., Zahouani, H., Loubet, J.L., Mathia, T.G. 1998, "Understanding and quantification of elastic and plastic deformation during a scratch test", Wear, Vol. 218, pp. 8-14.

Jin, M., Murakawa, M. 2001, "Development of a practical ultrasonic vibration cutting tool

system", Journal of Material Processing Technology, Vol. 113, pp. 342-347.
Kim, M., Park, Y.B., Okoli, O.I., Zhang, C. 2009, "Processing, characterization, and modeling of carbon nanotube-reinforced multiscale composites", Composites Science and Technology, Vol. 69, pp. 335-342.
Kimura, T., Ago, H., Tobita, M., Ohshima, S., Kyotani, M., Yumura, M. 2002, "Polymer Composites of Carbon Nanotubes Aligned by a Magnetic Field", Advanced Materials, Vol. 14, pp. 1380-1383.
Kumabe, J., Fuchizawa, K., Soutome, T., Nishimoto, Y. 1989, "Ultrasonic superposition vibration cutting of ceramics", Precision Engineering, Vol. 11, pp. 71-77.
Lam, D.C.C., Chong, A.C.M. 1999, "Indentation model and strain gradient plasticity law for glassy polymers", Journal of Materials Research, Vol. 14, pp. 3784-3788.
Ma, C.X., Shamoto, E., Moriwaki, T., Wang, L. 2004, "Study of machining accuracy in ultrasonic elliptical vibration cutting", Materials Science Forum, Vol. 471-472, pp. 396-400.
Ma, C.X., Shamoto, E., Moriwaki, T., Zhang, Y., Wang, L. 2005, "Suppression of burrs in turning with ultrasonic elliptical vibration cutting", International Journal of Machine Tools & Manufacture, Vol. 45, pp. 1295-1300.
Mahmoodi, M., Arjmand, M., Sundararaj, U., Park, S. 2012, "The electrical conductivity and electromagnetic interference shielding of injection molded mulit-walled carbon nanotube/polystyrene composites", Carbon, Vol. 50, pp. 1455-1464
Mahmoodi, M., Mostofa, M.G., Jun, M., Park, S.S. 2013, "Characterization and Micromilling of Flow Induced Aligned Carbon Nanotube Nanocomposites", Journal of Micro and Nano-Manufacturing, Vol. 1, pp. 011009-1-011009-8.
Malekian, M., Park, S.S., Jun, M.B.G. 2009, "Modeling of dynamic micro-milling cutting forces", International Journal of Machine Tools & Manufacture, Vol. 49, pp. 586-598
Malekian, M., Park, S.S., Strathearn, D., Mostofa, M.G., Jun, M.B.G. 2010, "Atomic force microscope probe-based nanometric scribing", Journal of Micromechanics and Mircoengineering, Vol. 20, pp. 1-11.
Malekian, M., Mostofa, M.G., Park, S.S., Jun, M.B.G. 2012, "Modeling of minimum uncut chip thickness in micro machining of aluminum", Journal of Materials Processing Technology, Vol. 212, pp. 533-559.
Miyake, K., Satomi, N., Sasaki, S. 2006, "Elastic modulus of polystyrene film from near surface to bulk measured by nanoindentation using atomic force microscopy", Applied Physics Letters, Vol. 89, pp. 031925-1-031925-3.
Moriwaki, T., Shamoto, E., Inoue, K. 1992, "Ultraprecision Ductile Cutting of Glass by Applying Ultrasonic Vibration", CIRP Annals – Manufacturing Technology, Vol. 41, pp. 141-144.
Nath, C., Rahman, M., Neo, K.S. 2009, "Machinability study of tungsten carbide using PCD tools under ultrasonic elliptical vibration cutting", International Journal of Machine Toools & Manufacture, Vol. 49, pp. 1089-1095.
Nix, W.D., Gao, H. 1998, "Indentation Size Effects in Crystalline Materials: A Law for Strain Gradient Plasticity", Journal of Mechanic and Physics of Solids, Vol. 46, pp. 411-425.
Oliver, W.C., Pharr, G.M. 1992, "An Improved Technique for Determining Hardness and Elastic Modulus Using Load and Displacement Sensing Indentation Experiments", Journal of Materials Research, Vol. 7, pp. 1564-1583.
Oliver, W.C., Pharr, G.M. 2004, "Measurement of hardness and elastic modulus by instrumented

indentation: Advances in understanding and refinements to methodology", Journal of Materials Research Vol. 19, pp. 3-20.
Pharr, G.M., Bolshakov, A. 2002, "Understanding nanoindentation unloading curves", Journal of Material Research Vol. 17, pp. 2660-2671.
Qian, D., Dickey, E.C., Andrews, R., Rantell, T. 2000, "Load Transfer and deformation mechanisms in carbon nanotube-polystyrene composites", Applied Physics Letters, vol. 76, pp. 2868-2870.
Sader, J.E., Chon, J.W., Mulvaney, P. 1999, "Calibration of rectangular atomic force microscope cantilevers". Review of Scientific Instruments, Vol. 70, pp. 3967-3969.
Samuel, J., Dikshit, A., DeVor, R.E., Kapoor, S.G., Hsia, K.J. 2009, "Effect of Carbon Nanotube (CNT) Loading on the Thermomechanical Properties and the Machinability of CNT-Reinforced Polymer Composites", Journal of Manufacturing Science and Engineering, Vol. 131, pp. 031008-1-031008-9.
Samuel, J., Kapoor, S.G., DeVor, R.E., Hsia, K.J. 2010, "Effect of Microstructural Parameters on the Machinability of Aligned Carbon Nanotube Composites", Journal of Manufacturing Science and Engineering, Vol. 132, pp. 051012-1-051012-9.
Shamoto, E., Moriwaki, T. 1994, "Study on Elliptical Vibration Cutting", CIRP Annals – Manufacturing Technology, Vol. 43, pp. 35-38.
Shamoto, E., Moriwaki, T. 1999, "Ultraprecision diamond Cutting of Hardened Steel by Applying Elliptical Vibration Cutting", CIRP Annals – Manufacturing Technology, Vol. 48, pp. 441-444.
Shamoto, E., Moriwaki, T. 2002, "Development of Ultrasonic Elliptical Vibration Controller for Elliptical Vibration Cutting", CIRP Annals – Manufacturing Technology, Vol. 51, pp. 327-330.
Skelton, R.C. 1968, "Turning with an oscillating tool", International Journal of Machine Tools Design and Research, Vol. 8, pp. 239-259.
Spitalsky, Z., Tasis, D., Papagelis, K., Galiotis, C. 2010, "Carbon nanotube-polymer composites: Chemistry, processing, mechanical and electrical properties", Progress in Polymer Science, Vol. 35, pp. 357-401.
Thostenson, E., Chou, T.-W. 2002, "Aligned multi-walled carbon nanotube-reinforced composites: processing and mechanical characterization", Journal of Physics D: Applied Physics, Vol. 35, pp. L77-L80.
Waldorf, D.J. 2006, "A Simplified Model for Plowing Forces in Turning", Journal of Manufacturing Processes, Vol. 8, pp. 76 - 82
Xia, Z.H., Lou, J., Curtin, W.A. 2008, "A multiscale experiment on the tribological behavior of aligned carbon nanotube/ceramic composites", Scripta Materialia, Vol. 58, pp. 223-226.
Yang, Z., Dong, b., Huang, Y., Liu, L., Yan, F.Y., Li, H.L. 2005, "Enhanced wear resistance and miro-hardness of polystyrene nanocomposites by carbon nanotubes", Materials and Physics, Vol. 94, pp. 109-113.
Yu, M.F., Lourie, O., Dyer, M.J., Moloni, K., Kelly, T.F., Ruoff, R.S. 2000, "Strength and Breaking Mechanism of Multiwalled Carbon Nanotubes Under Tensile Load", Science, Vol. 287, pp. 637–640.